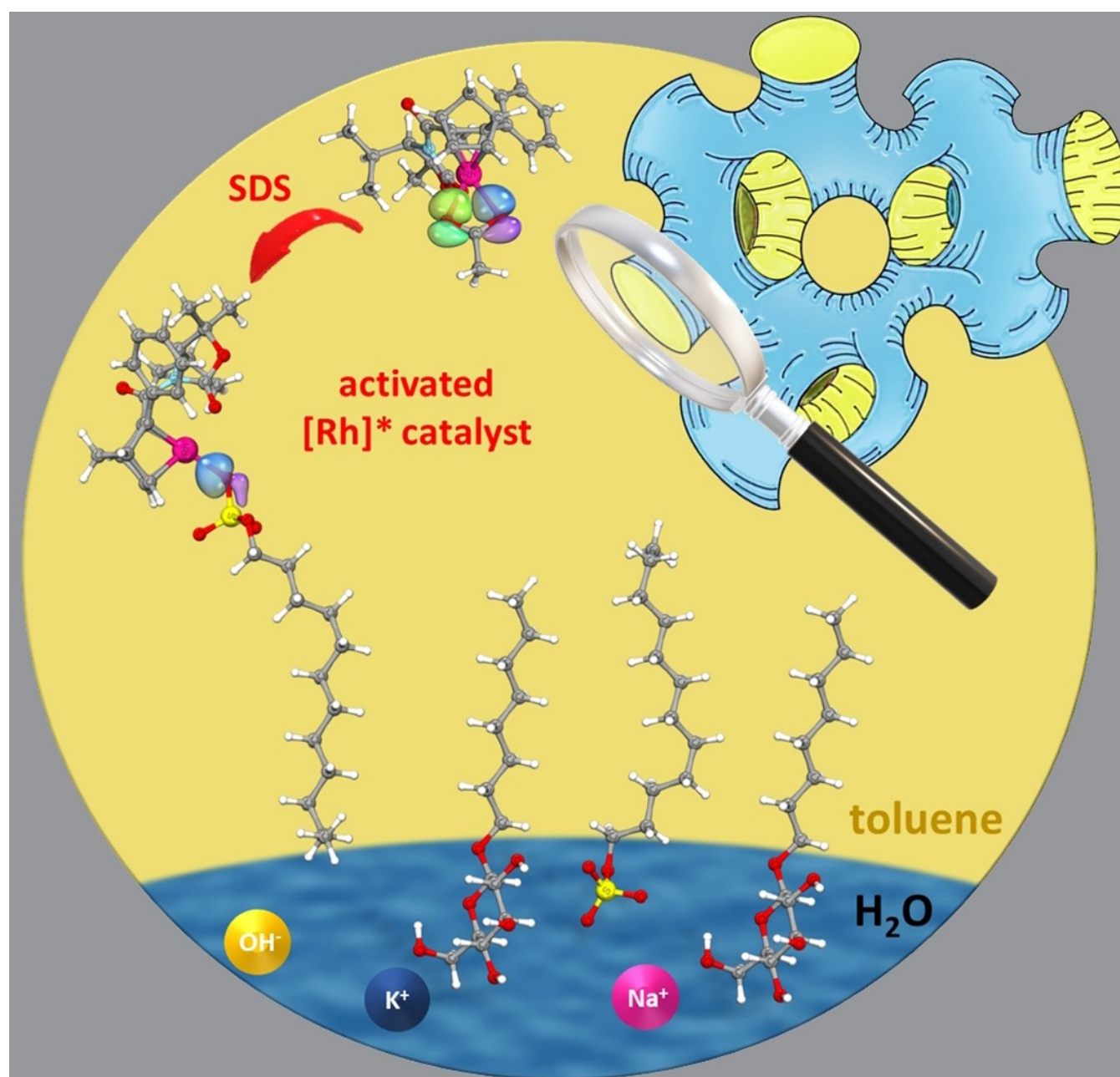Special
Issue

Interplay of Polarity and Confinement in Asymmetric Catalysis with Chiral Rh Diene Complexes in Microemulsions

Manuel Kirchhof+,[a] Karina Abitaev+,[b] Abdulwahab Abouhaileh,[b] Katrin Gugeler,[c] Wolfgang Frey,[a] Anna Zens,[a] Johannes Kästner,*[c] Thomas Sottmann,*[b] and Sabine Laschat*[a]

Abstract: Microemulsions provide a unique opportunity to tailor the polarity and liquid confinement in asymmetric catalysis via nanoscale polar and nonpolar domains separated by a surfactant film. For chiral diene Rh complexes, the influence of counterion and surfactant film on the catalytic activity and enantioselectivity remained elusive. To explore this issue chiral norbornadiene Rh(X) complexes (X = OTf, OTs, OAc, PO_2F_2) were synthesized and characterized by X-ray crystallography and theoretical calculations. These complexes were used in Rh-catalyzed 1,2-additions of phenylboroxine to N-tosylimine in microemulsions stabilized either exclusively by n-octyl-β-D-glucopyranoside (C_8G_1) or a C_8G_1-film doped with anionic or cationic surfactants (AOT, SDS and DTAB). The Rh(OAc) complex showed the largest dependence on the composition of the microemulsion, yielding up to 59% (90%ee) for the surfactant film doped with 5 wt% of AOT as compared to 52% (58%ee) for neat C_8G_1 at constant surfactant concentration. Larger domains, determined by SAXS analysis, enabled further increase in yield and selectivity while the reaction rate almost remained constant according to kinetic studies.

Introduction

Confined reaction spaces provided by micelles and microemulsions have received much attention during the last years.[1–12] Compared to micellar systems, microemulsions are mixtures of two (or more) immiscible solvents, usually at least one polar and one nonpolar, separated at the nanoscale by an amphiphilic film, often consisting of surfactants, which makes them thermodynamically stable. In both micellar systems and microemulsions, an amphiphilic film forms after the monomeric solubility in the solvent is exceeded, i.e. above the critical micelle concentration (CMC). While in the former systems differently shaped empty micelles exist, microemulsions excel through the multitude of variously shaped swollen micelles as well as network- or sponge-like bicontinuous structures in which polar and nonpolar domains are simultaneously present in a thermodynamically stable manner.[8,13] The outstanding properties of both reaction media are their large interfacial area, adjustable by the surfactant concentration, and the ability to solubilize nonpolar or/and polar reactants in either normal or inverse micelles, or in the polar and nonpolar domains of the microemulsion. Thus, very high reaction rates can be attained in both micellar systems and microemulsions.

However, the two types of reaction media differ on the one hand in the local concentration of the reactants and on the other hand in the environment in which the catalyst complex is located.[14,15] While in micellar reaction media the concentration of reactants is strongly limited by their solubility in the micellar core, the nanoscale solvent domains in microemulsions allow the reactant concentration to be adjusted over a wide concentration range. Assuming a slightly amphiphilic catalyst complex, the catalyst is localized in the surfactant film, where the hydrophobic part of the catalyst in the micellar system interacts only with the hydrophobic alkyl chains, while due to the penetration of solvent molecules into the surfactant film in microemulsions the catalyst environment and therewith the interaction is significantly different. Note that the surfactant film in micellar systems is strongly curved, while its curvature in microemulsions is considerably lower and adjustable suggesting an impact on the orientation of the catalyst complex. Last but not least, the adjustable phase behaviour of both reaction media, but especially of the microemulsions, can be used for product separation and catalyst recycling, as shown for example in the three-step synthesis of the fungicide boscalid®.[16]

The multifarious and adjustable nanostructure of microemulsions provides well defined nanoreactors to control the morphology and topology of copolymers,[1] inorganic and metal nanoparticles,[2,3] metal–organic frameworks (MOFs),[4] to tailor dynamics of proteins[5] and dyes[6] and to gain more general insight into structure and phase behaviour of such complex fluids.[7] Furthermore, the nanometer-sized domains of hydrophilic and hydrophobic solvents inside microemulsions[8] have been successfully used to accelerate stoichiometric and catalytic reactions of small molecules.[9,10] In contrast, only a few studies have dealt with asymmetric catalysis in microemulsions, such as vitamin B12-catalyzed isomerization of cyclopentenol,[10] Au-catalyzed lactonization of allenic acids[11] and asymmetric Ru-catalyzed transfer-hydrogenation of ketones.[12]

Recently, we investigated the effect of nanoscale confinement comprising a highly dynamic amphiphilic surfactant film by means of the Rh-catalyzed asymmetric 1,2-addition of triphenylboroxine to N-tosylimines utilizing chiral Rh-diene

[a]   M. Kirchhof,[+] Dr. W. Frey, Dr. A. Zens, Prof. S. Laschat
      Institut für Organische Chemie
      Universität Stuttgart
      Pfaffenwaldring 55, 70569 Stuttgart (Germany)
      E-mail: sabine.laschat@oc.uni-stuttgart.de

[b]   K. Abitaev,[+] A. Abouhaileh, Prof. T. Sottmann
      Institut für Physikalische Chemie
      Universität Stuttgart
      Pfaffenwaldring 55, 70569 Stuttgart (Germany)
      E-mail: t.sottmann@ipc.uni-stuttgart.de

[c]   K. Gugeler, Prof. J. Kästner
      Institut für Theoretische Chemie
      Universität Stuttgart
      Pfaffenwaldring 55, 70569 Stuttgart (Germany)
      E-mail: kaestner@theochem.uni-stuttgart.de

[+]   These authors contributed equally to this work.

      Supporting information for this article is available on the WWW under
      https://doi.org/10.1002/chem.202102752

      Part of a Special Issue on Contemporary Challenges in Catalysis.

Chemistry–A European Journal

Full Paper
doi.org/10.1002/chem.202102752

**Chemistry Europe**
European Chemical
Societies Publishing

complexes in microemulsions.[17,18] Rh-diene complexes were chosen as benchmark catalysts because they are very versatile and catalyse a large variety of reactions.[19,20] Furthermore they are rather slow in conventional solvents such as dioxane.[18] Interestingly, we found that both the yield and reaction rate significantly improved in the microemulsion, which we explained by its large interfacial area and its ability to solubilize both nonpolar reactants as well as the polar KOH needed for the activation of the Rh-diene complex.

During our previous studies we noticed that the catalytic performance depended strongly on the polarity and steric and electronic effects of the diene ligand.[18] Moreover, monomeric neutral and cationic Rh-diene complexes differed significantly from their dimeric counterparts regarding enantiocontrol in microemulsions vs. conventional solvents.[17] Therefore, we surmised that the type of counterion bound to the Rh complex and thus the charge density at the Rh centre might control the outcome of the catalytic reaction. Thus, we aimed to investigate the role of the polarity of the catalyst by variation of the counterion. Secondly, based on the assumption that the catalyst complex is located in or near the previously non-ionic surfactant film, the question arose whether and how the interaction of the catalyst with the film effects the catalytic reaction. Therefore, by doping the non-ionic film with ionic surfactants, we wanted to investigate the influence of a charged confinement on the yield, selectivity and reaction rate. And finally, we planned to vary the concentration of the ionic/non-

ionic surfactant mixture to find out the influence of the size of the liquid confinement given by the water and oil domains of the microemulsion on the catalytic reaction. These studies will clarify whether highly dynamic microemulsions actually provide nanostructured confined reaction spaces similar to mesoporous solids or whether it is more akin to another solvent for Rh-diene catalysis. As discussed below, in the current manuscript we will investigate the influence of the use of microemulsion stabilized by different amphiphilic films as reaction media on the enantioselectivity and yield of the Rh-catalyzed 1,2-addition of triphenylboroxine **2** to *N*-tosylimine **1** (Scheme 1). Therefore, we will use rhodium complexes with different anions [Rh(**L2**)X] (X = OTf, OTs, OAc, PO$_2$F$_2$) in C$_8$G$_1$-based microemulsions either doped with cationic dodecyltrimethylammonium bromide (DTAB), anionic sodium dodecyl sulfate (SDS) or anionic dioctyl sodium sulfosuccinate (AOT) as co-surfactant and evaluate the results with regard to the nanostructure of the microemulsion and the polarity of the amphiphilic film.

Results and Discussion

In the following we will first describe the synthesis of the Rh-diene complexes and the characterization of their solid-state structure obtained by X-ray crystal structure analysis and theoretical calculations. Afterwards, the phase behaviour of the microemulsions that were used as reaction media will be shown
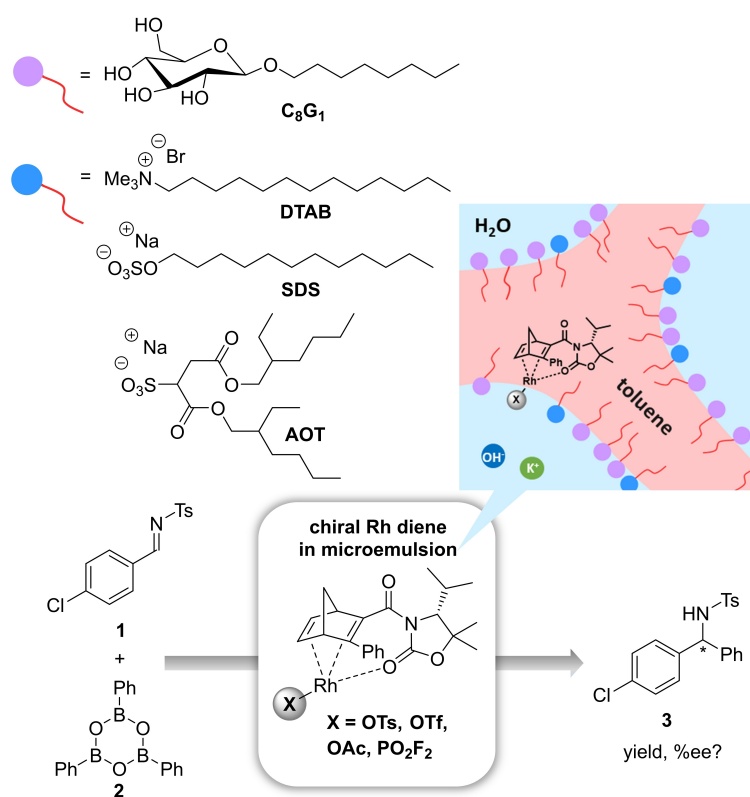
Scheme 1. Rh-catalyzed 1,2-addition in C$_8$G$_1$-based microemulsions doped with co-surfactants. For easier comparison the following abbreviations will be used: SDS = sodium dodecylsulfate; SDS$^-$ = dodecylsulfate anion; AOT = dioctyl sodium sulfosuccinate; AOT$^-$ = dioctyl sulfosuccinate anion; DTAB = dodecyltrimethylammonium bromide; DTAB$^+$ = dodecyltrimethylammonium cation.

Chemistry–A European Journal

Full Paper
doi.org/10.1002/chem.202102752

Chemistry Europe
European Chemical
Societies Publishing

particularly concentrating on the influence of ionic co-surfactants on the phase diagram. Subsequently, the performance of the Rh-diene complexes in the 1,2-addition in microemulsions doped with anionic co-surfactants will be discussed and compared to the catalysis in dioxane. Eventually, the dependence of kinetics on the temperature and the chosen reaction medium will be investigated.

Synthesis, solid state structures and DFT calculations of Rh-diene complexes

Known dimeric Rh complex [Rh(**L2**)Cl]$_2$[18] (Scheme 2) was treated with 1 equiv. of AgSbF$_6$ in CH$_2$Cl$_2$ as described previously[17] to give the corresponding dimeric complex [(Rh(**L2**))$_2$Cl]SbF$_6$.[17] However, when [Rh(**L2**)Cl]$_2$ was treated with 2 equiv. of AgSbF$_6$ the dimer was cleaved and cationic [Rh(**L2**)OH$_2$]SbF$_6$ was obtained in quantitative yield.

To obtain monomeric Rh complexes with different counterions, dimeric Rh complex [Rh(**L2**)Cl]$_2$ was treated with 2 equiv. of Ag(I) salts to yield [Rh(**L2**)X] (X = OTf, OTs, OAc) respectively. Treatment of [Rh(**L2**)Cl]$_2$ with 2 equiv. of AgPF$_6$ led to the formation of [Rh(**L2**)PO$_2$F$_2$] due to hydrolysis of the PF$_6^-$ anion. This exceptional behaviour was previously described in literature[21,22] for anion exchanges in palladium and rhodium complexes. It is caused by residual water in the silver salt that leads to a silver-catalyzed hydrolysis of PF$_6^-$.
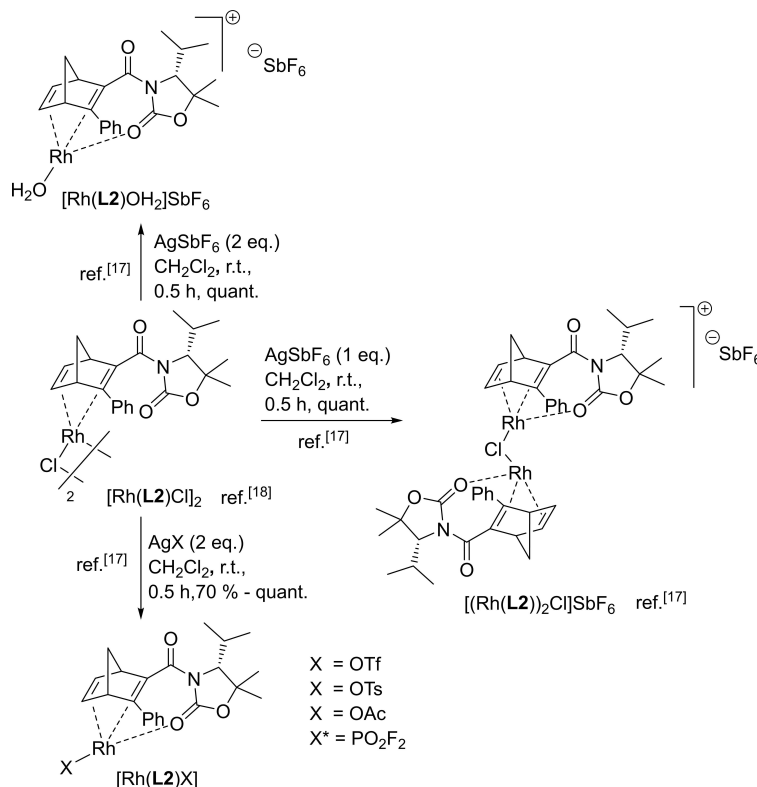
All prepared complexes [Rh(**L2**)X] (X = OTf, OTs, OAc, PO$_2$F$_2$) and [Rh(**L2**)OH$_2$]SbF$_6$ readily crystallized as yellow needles that were suitable to obtain X-ray crystal structures (Figure 1 and Figure 2).

In all monomeric complexes [Rh(**L2**)X] the anion is part of the inner sphere and the rhodium central atom is coordinated by either one (X = OTf, OTs, PO$_2$F$_2$) or two (X = OAc) oxygens from the anion (Figure 1). The residual coordination sites of the square planar complexes are occupied with the carbonyl oxygen of the oxazolidinone moiety and the diene. For the cationic complex [Rh(**L2**)OH$_2$]SbF$_6$ the weakly coordinating anion SbF$_6^-$ is located in the outer sphere and the free coordination site is occupied with an additional water molecule (Figure 2).

This observation is in good agreement with our previous results for the similar complex [Rh(**L1**)OH$_2$]SbF$_6$ (Scheme S1, Supporting Information).[17]

A comparison of crystallographic data of the monomeric complexes [Rh(**L2**)X] (X = OTf, OTs, OAc, PO$_2$F$_2$) and [Rh(**L2**)OH$_2$] SbF$_6$ is given in Table 1.

For all neutral complexes [Rh(**L2**)X] (X = OTf, OTs, OAc, PO$_2$F$_2$) the C=C bond length is in the same range (between 1.392(5) Å and 1.398 Å). Only the C10=C11 bond in the cationic complex [Rh(**L2**)OH$_2$]SbF$_6$ is slightly elongated (1.403 Å). Furthermore, the bond distances of the rhodium atom and the oxygen of the respective anion is similar for [Rh(**L2**)OTs], [Rh(**L2**)PO$_2$F$_2$] and [Rh(**L2**)OTf] (between 2.072 Å and 2.114 Å). However, the distance is much higher for [Rh(**L2**)OAc] (2.231 Å

Scheme 2. Synthesis of rhodium complexes [Rh(**L2**)X] (X = OTf, OTs, OAc, PO$_2$F$_2$) and [Rh(**L2**)OH$_2$]SbF$_6$ with different anions.

Chemistry–A European Journal

Full Paper
doi.org/10.1002/chem.202102752

Chemistry
Europe
European Chemical
Societies Publishing
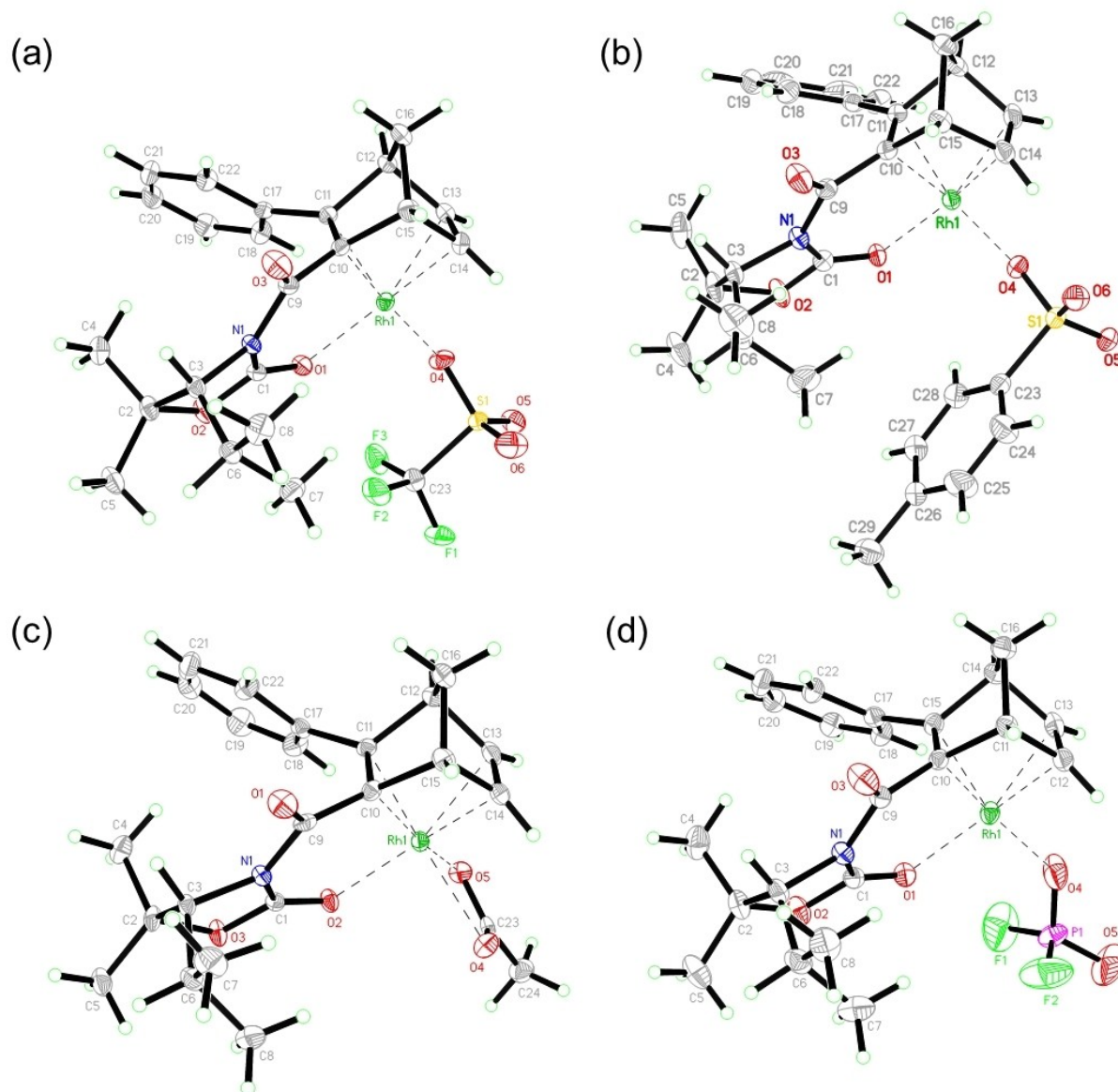
Figure 1. Solid state structures of the monomeric complexes [Rh(**L2**)X] (X=OTf (a), OTs (b), OAc (c), PO$_2$F$_2$ (d)). Selected bond distances, bond angles, tilt angles and bite angles are compared in Table 1.

and 2.342 Å) where the acetate anion binds in a bidentate fashion.

For a better understanding of the binding situation between the rhodium and the respective anion DFT calculations at the B3LYP-D3(BJ)/def2-SVP level were performed with the dioxane solvent described by the conductor-like screening model (COSMO) in Turbomole.[23] The minimized structures are in excellent agreement with the crystal structure data (Figure 3).

The intrinsic bond orbitals (IBOs)[24] responsible for the bond between Rh and the counterions are depicted in Figure 3. These are primarily p-orbitals at the oxygen atoms of the ligands, polarized towards the Rh centre. The polarization can be quantified by the fraction of the charge of these intrinsic bond orbitals located at rhodium, which ranges from 8.4% for TfO to

10.1% for PO$_2$F$_2$. Acetate provides two orbitals with 7.9% and 9.0% of their charge at Rh and thus forms the strongest bond.

Additionally, the IBOs of Rh(**L2**) complexes with an SDS$^-$ and AOT$^-$ counterion were calculated after initial geometry optimization (Figure 4).

The IBOs of the bond between the Rh and the SDS$^-$ or respectively AOT$^-$ counterion are similar to the IBOs shown in Figure 3. Again, a polarization of the p-orbitals of the oxygen towards the Rh is observed for both counterions. The fraction of charge located at the Rh is 8.6% for SDS$^-$ and 10.3% for AOT$^-$. Therefore, these IBOs are also quantitatively comparable to the IBOs in Figure 3.

The IBOs match well with the calculated binding energies of the Rh–X bonds, which are strongest for acetate (372.6 kJ mol^{-1}), while they are 269.1 to 307.4 kJ mol^{-1} for the
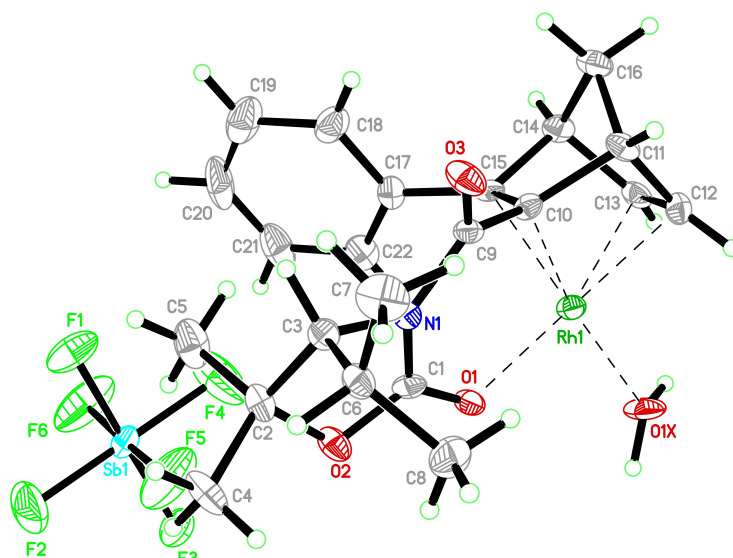
Chemistry–A European Journal

Full Paper
doi.org/10.1002/chem.202102752

Chemistry Europe
European Chemical
Societies Publishing

Figure 2. Solid state structure of the cationic complex [Rh(**L2**)OH₂]SbF₆. Selected bond distances, bond angles, tilt angles and bite angles are compared to the neutral complexes in Table 1.

Table 1. Comparison of bond distances, bond angles, tilt angles and bite angles of monomeric complexes [Rh(**L2**)X] (X = OTf, OTs, OAc, PO₂F₂) and [Rh(**L2**)OH₂]SbF₆.

	neutral complexes [Rh(L2)OTf]	[Rh(L2)OAc]	[Rh(L2)OTs]	[Rh(L2)PO₂F₂]	cationic complex [Rh(L2)OH₂]SbF₆
C=C (distance)/Å	C10=C11 1.423(4)	C10=C11 1.448(5)	C10=C11 1.431(5)	C10=C11 1.426(4)	C10=C11 1.422(7)
	C13=C14 1.395(4)	C13=C14 1.398(6)	C13=C14 1.392(5)	C13=C14 1.397(5)	C13=C14 1.403(8)
Rh→C=C (av.distance)/Å	C10=C11 2.049(3)	C10=C11 2.034(4)	C10=C11 2.055(3)	C10=C11 2.049(3)	C10=C15 2.043(5)
	C13=C14 2.119(3)	C13=C14 2.114(4)	C13=C14 2.115(3)	C13=C14 2.109(3)	C13=C14 2.112(5)
tilt angle/deg	C10-C11-C13-C14 −0.5(2)	C10-C11-C13-C14 −0.8(3)	C10-C11-C13-C1 −0.4(3)	C10-C11-C13-C14 −0.4(3)	C10-C11-C13-C14 −1.3(4)
bite angle/deg	C10-Rh1-C13 81.6(1)	C10-Rh1-C13 82.0(2)	C10-Rh1-C13 81.9(1)	C10-Rh1-C13 82.1(1)	C10-Rh1-C13 82.1(2)
Rh→X/Å	Rh1→O4: 2.114(2)	Rh1→O4: 2.342(3) Rh1→O5: 2.231(3)	Rh1→O4: 2.087(2)	Rh1→O4: 2.072(3)	Rh1→F: (> 4 Å)
Rh→1O=C/Å	2.094(2)	2.090(3)	2.087(2)	2.109(2)	2.079(3)
Rh→OH₂/Å	–	–	–	–	2.100(4)
C=O1/Å	1.229(3)	1.226(4)	1.225(4)	1.220(4)	1.227(6)

other ligands (Table 2). It should be emphasized that surfactant anions SDS⁻ and AOT⁻ are much weaker bound to Rh as compared to acetate. In particular AOT⁻ (and OTf) possessed the weakest binding energy.

Phase behavior of the microemulsion doped with ionic surfactants

In order to answer the question whether and how the interaction of a polar catalyst with the amphiphilic surfactant

Table 2. Binding energies for the Rh complexes with different counterions.

Rh complex	Binding energy/kJ mol⁻¹
[Rh(**L2**)OAc]	372.6
[Rh(**L2**)OTf]	270.0
[Rh(**L2**)OTs]	307.4
[Rh(**L2**)PO₂F₂]	293.9
[Rh(**L2**)SDS]	293.8
[Rh(**L2**)AOT]	269.1

Chemistry–A European Journal

Full Paper
doi.org/10.1002/chem.202102752

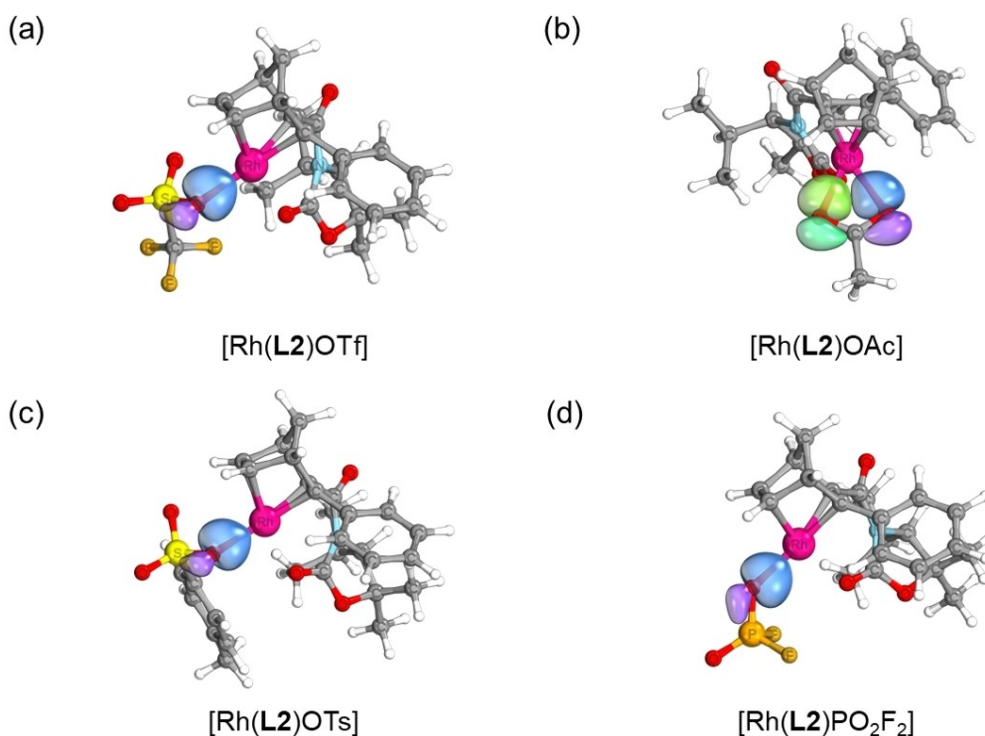**Chemistry Europe**
European Chemical
Societies Publishing

Figure 3. Intrinsic bonding orbitals between Rh(**L2**) and different anions. These are oxygen p-orbitals polarized strongly towards Rh. The strongest polarization of a single orbital is found for PO$_2$F$_2$, while the strongest overall bond is found for the bidentate acetate.
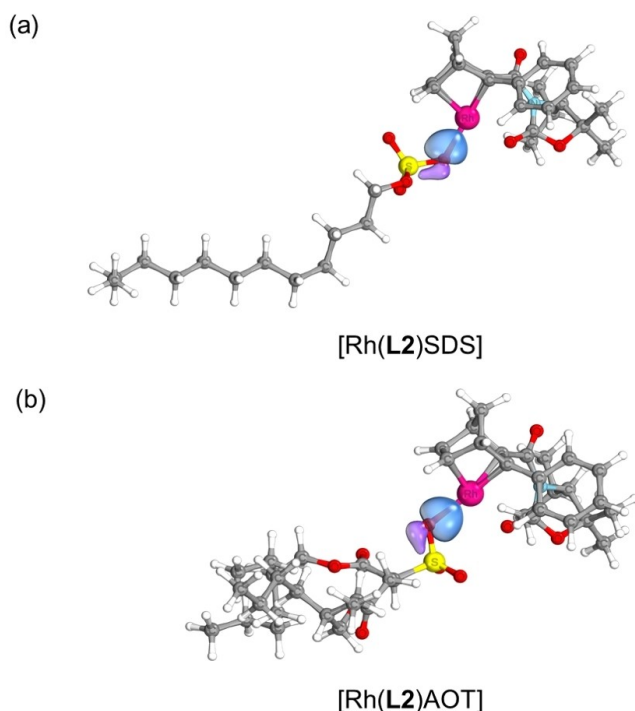

Figure 4. Intrinsic bonding orbitals between Rh(**L2**) and SDS$^-$ (a) and AOT$^-$ (b). These are oxygen p-orbitals polarized strongly towards Rh.

film effects the yield and selectivity of the Rh-catalyzed asymmetric 1,2-addition of triphenylboroxine **2** to *N*-tosylimine

1, we started from the microemulsion used in our previous studies[17,18] and replaced the non-ionic sugar surfactant C$_8$G$_1$ partially by the anionic surfactants SDS and AOT. Due to the fact that microemulsions are only stable in a limited temperature and composition range, their phase behaviour must be thoroughly investigated. Starting point for these studies was the $T(\gamma)$-phase diagram of the system H$_2$O/KOH, toluene, C$_8$G$_1$, *N*-tosylimine **1** and triphenylboroxine **2**. This so-called $T(\gamma)$-section through the phase prism was recorded as a function of temperature and surfactant concentration γ using equal masses of H$_2$O/KOH and toluene ($\alpha = 50$ wt%), 0.33 wt% of KOH in the H$_2$O/KOH-mixture ($\varepsilon = 0.33$ wt% (12.9 μL, 3.1 M KOH)), 0.24 mmol of **2** and 0.20 mmol **1**. Note, that along this section, the mass fraction S of the two reactants in the surfactant/reactant mixtures is kept constant at $S = 11$ wt%. As can be seen in the Supporting Information (Figure S1), the phase diagram recorded in this work is in almost quantitative agreement with previous results.[18]

Based on this microemulsion, the non-ionic amphiphilic film was stepwise doped with the anionic SDS keeping all other parameters constant, i.e., $\alpha = 50$ wt%, $\varepsilon = 0.33$ wt% and $S = 11$ wt%. As shown in Figure 5, left, replacing only 5 wt% of C$_8$G$_1$ by SDS (■), specified by the concentration δ_{SDS} of SDS in the C$_8$G$_1$/SDS mixture, shifts the phase boundaries to lower surfactant concentrations γ and thus allows a much more efficient solubilization of H$_2$O/KOH and toluene. The $\tilde{X}$-point, which is measure of phase inversion temperature and efficiency, is located at $\tilde{T} = 35.0 \pm 0.5$ °C and $\tilde{\gamma} = 15.4 \pm 0.5$ wt%. A similar effect was observed and studied by Kaler et al. who
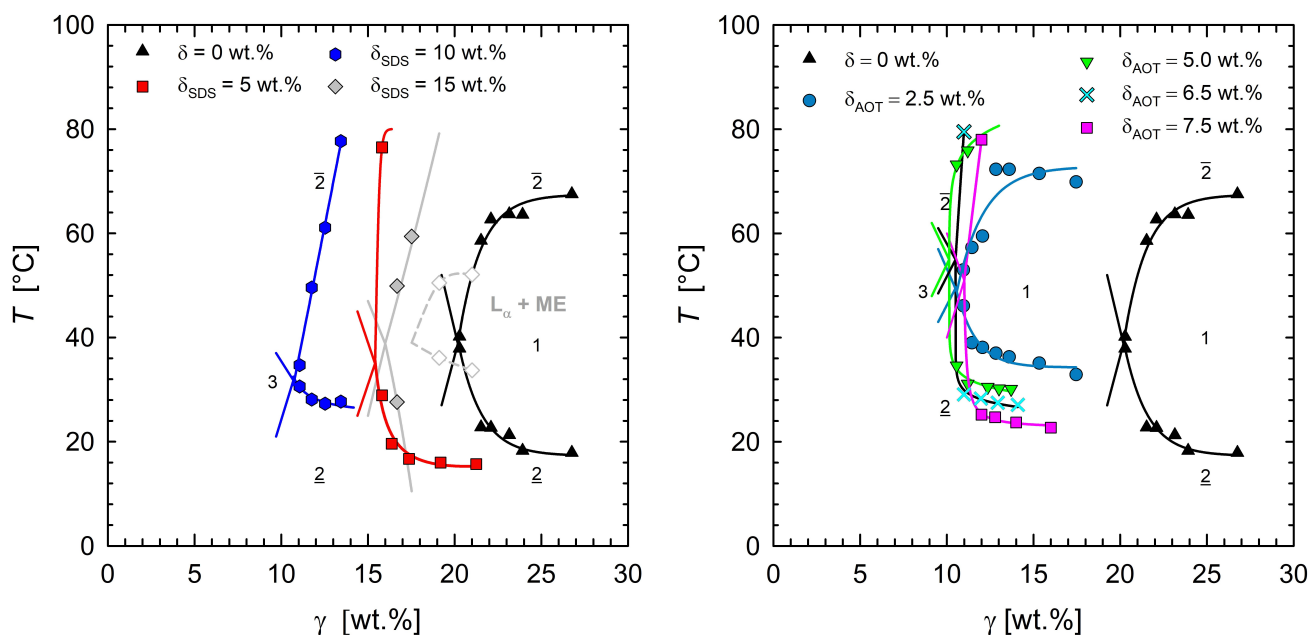
Chem. Eur. J. **2021**, *27*, 16853–16870   www.chemeurj.org

16859

© 2021 The Authors. Chemistry - A European Journal published by Wiley-VCH GmbH

Chemistry–A European Journal

Full Paper
doi.org/10.1002/chem.202102752

Chemistry Europe
European Chemical
Societies Publishing

Figure 5. $T(\gamma)$-sections of the system H_2O/KOH-toluene-C_8G_1/SDS (*left*)/ AOT (*right*)-triphenylboroxine **2**/ *N*-tosylimine **1** at $\alpha = 50$ wt%, $\varepsilon_{KOH} = 0.33$ wt%, $S = 11$ wt% at various co-surfactant concentrations δ of SDS and AOT in the surfactant mixture. Increasing δ_{SDS} stepwise, the phase boundaries shift at first to smaller γ values ($\delta_{SDS} \leq 10$ wt%). With further increasing δ_{SDS} this trend turns around. The phase boundaries shift back towards higher γ and a coexistence region of microemulsion and lamellar phase (dashed line) was observed. Using AOT instead of SDS a similar trend was found. However, significantly lower concentrations δ_{AOT} of AOT in the AOT/C_8G_1 mixture were sufficient to allow for an even slightly larger shift of the phase boundaries to smaller γ values.

found a strong increase in efficiency to form a microemulsion by replacing small amounts of the non-ionic surfactant triethoxy monooctylether (C_8E_3) by the cationic surfactant didodecyl dimethyl ammonium bromide (DDAB).[25] They as well as others[26] reasonably argued that the enhanced efficiency of the ionic/non-ionic surfactant mixture can be attributed to the electrostatic interactions within the amphiphilic film introduced by the addition of the ionic surfactant, resulting in an electro-static stiffening of the surfactant film, which was shown to reduce their thermal fluctuation.[25,27] Thus, a higher amount of water and oil can be solubilized. Furthermore, a steeper upper phase boundary as well as the broadening of the one-phase region can be observed, which are a consequence of the inverse temperature-dependent phase behavior of ionic and non-ionic microemulsions,[28] so that these temperature trends compensate. In contrast, the lower phase boundary is slightly shifted to lower temperatures. The trends observed for $\delta_{SDS} = 5$ wt% continue when 10 wt% of C_8G_1 is replaced with SDS (●). The phase boundaries shift further to lower surfactant concentrations ($\tilde{\gamma} = 10.7 \pm 0.5$ wt%) and the upper phase boundary becomes steeper. However, a further increase of the SDS concentration in the SDS/C_8G_1 mixture to $\delta_{SDS} = 15$ wt% (♦) causes a reversal of the trends. The phase boundaries shift back to larger surfactant concentrations and a two-phase region appears, in which a lamellar phase coexists with the micro-emulsion (L$_\alpha$ + ME, dashed line). While the latter is a result of the continuous suppression of the thermal fluctuations of the surfactant film, the former might be related to the decreasing distance between the SDS$^-$ headgroups and the increasing number of Na$^+$ counterions.

The second anionic surfactant used to investigate the influence of a charged amphiphilic surfactant film on the yield and selectivity of Rh-catalyzed asymmetric 1,2-addition of triphenylboroxine **2** to *N*-tosylimine **1** was AOT (Figure 5, right). Due to its two branched tails, the efficiency of AOT to solubilize water and oil in a microemulsion is greater than that of SDS. In this context, the initial co-surfactant mass ratio of AOT was chosen to $\delta_{AOT} = 2.5$ wt% (●). The presence of this small amount of AOT increases the efficiency of the surfactant mixture significantly to $\tilde{\gamma} = 10.5 \pm 0.5$ wt%. This significantly larger positive effect of AOT on the solubilization efficiency results due to its larger alkyl moiety and its branched structure on the one hand, and a larger degree of dissociation of Na$^+$ counterions on the other hand. A further replacement of C_8G_1 with AOT to $\delta_{AOT} = 5.0$ wt% (▼) and $\delta_{AOT} = 6.5$ wt% (×), has almost no effect on the surfactant mixture efficiency, whereas for $\delta_{AOT} = 7.5$ wt% (■), as for SDS, a slight shift of the phase boundaries towards higher surfactant concentrations was observed most probably related to the decreasing distance between the AOT headgroups and the increasing number of Na$^+$ counterions.[25]

To study, whether an inversely charged amphiphilic film has a different influence on the performance of the catalytic reaction, the non-ionic C_8G_1-based microemulsion was doped with the cationic surfactant DTAB. Contrary to SDS and AOT, replacing 5 wt% of C_8G_1 with DTAB the phase boundaries were shifted to higher surfactant concentrations. By increasing the DTAB concentration further to 10 wt% the efficiency of the surfactant mixture was slightly higher than the non-doped system, see the Supporting Information (Figure S2). These

Chemistry–A European Journal

Full Paper
doi.org/10.1002/chem.202102752

Chemistry Europe
European Chemical
Societies Publishing

results suggest that DTAB is less dissociated in the dilute KOH aqueous domains than the anionic surfactants SDS and AOT so that the hydroxide ions are able to shield the electrostatic interactions of the DTAB$^+$ molecules. Hence, to proof this explanation, the KOH mass fraction in water was reduced by half to reduce the shielding of the electrostatic interactions. As a consequence, a significant shift of the phase boundaries to lower γ was found (see Figure S2 in the Supporting Information) as observed for the two anionic surfactants at higher concentrations of KOH.

The possibility to increase the efficiency of the surfactant mixture allowed us to reduce the surfactant amount utilized for the catalytic reaction considerably. Moreover, since the surfactant amount is inversely proportional to the length scale of the bicontinuous structure and proportional to the total specific interface S/V generated by the amphiphilic film, we were able to study the influence of these parameters on the catalytic performance of this nanostructured reaction media. To quantify the length scale of the structure and its specific interface, SAXS experiments were exemplary performed at the European Synchrotron Radiation Facility (ESRF, Grenoble, France) by means of selected microemulsions doped with AOT. Scattering curves of the starting microemulsion ($\delta = 0$ wt% and $\gamma = 28$ wt%) and two microemulsions containing 5 wt% AOT in the C_8G_1/AOT mixture but different surfactant concentrations of $\gamma = 14$ wt% and 21 wt% were recorded at $T = 60\,°C$. The corresponding scattering intensities $I(q)$ were plotted as a function of the scattering vector q in Figure 6 using a double logarithmic representation together with the phase diagrams of the respective microemulsion systems (inlet Figure 6). All curves show the typical features expected for the scattering of bicontinuous microemulsions. At low q, an almost constant intensity is observed, which with increasing q, starts to rise until a scattering peak is reached. In the middle q region, the scattering decreases continuously showing especially for the AOT-doped microemulsions a scattering shoulder at $2q_{max}$, which arises from multiple scattering. Increasing q further the scattering finally converges towards the incoherent background. Thereby the slope of the decay at high q-values results from a combination of the so-called film (q^{-2} decay) and bulk contrast (q^{-4} decay)[29] contributions.

As can be seen, the position of the scattering peak significantly shifts towards smaller q-values when the surfactant concentration is decreased from $\gamma = 28$ wt% to 14 wt%. This shift corresponds to an increasing size of the water- and toluene-rich domains caused by the significantly lowered number of surfactant molecules available to form the amphiphilic film on the nanoscale. Analysing the low and middle q region with the Teubner-Strey (TS) model[30] and considering multiple scattering,[31,32] (solid line), an increase of the domain size $d_{TS}/2$ by a factor of almost 2.5 from 42 Å to 103 Å was obtained when the surfactant concentration is decreased from $\gamma = 28$ wt% to 14 wt% (Table 3). Furthermore, the correlation length ξ_{TS}, which is a measure of the long-range order and the film-film correlation increases in the same order of magnitude from $\xi_{TS} = 43$ Å to 107 Å.
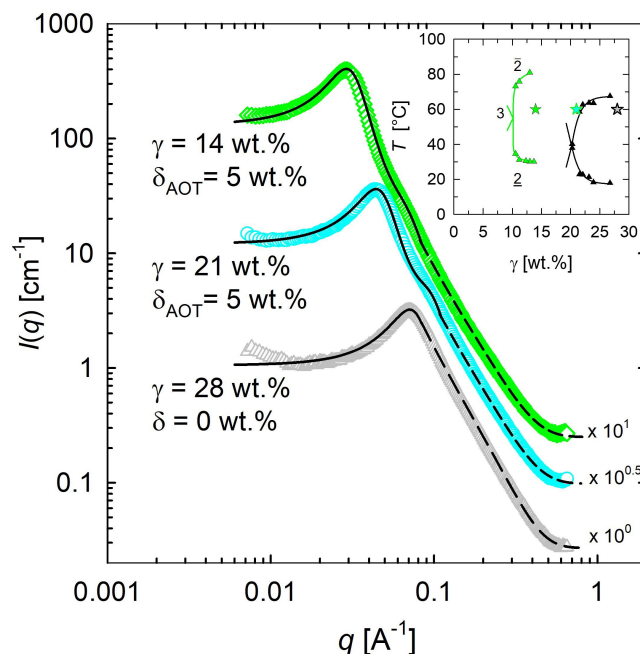

Figure 6. SAXS curves of H_2O/KOH-toluene-C_8G_1/AOT-triphenylboroxine **2**/N-tosylimine **1** recorded at $\gamma = 28$ wt% ($\delta = 0$ wt%, grey), 21 wt% and 14 wt% ($\delta_{AOT} = 5$ wt%, green and cyan) and $T = 60\,°C$. Note that the scattering curves are displaced by a factor of 10^x. The solid lines represent the fits using the Teubner-Strey model,[30] with considering multiple scattering[31,32], the dashed lines correspond to Porod-fits using a combination of bulk and film contrast scattering.[29] The inset shows the corresponding $T(\gamma)$-sections with the SAXS compositions (stars).

Table 3. Size of water/oil domains $d_{TS}/2$, correlation lengths ξ_{TS} and specific interface S/V obtained from the analysis of the SAXS-curves by the Teubner-Strey model,[30] considering multiple scattering[31,32] and the Porod analysis of the high q scattering intensity[29] for the respective microemulsion compositions.

γ [wt. %]	δ_{AOT} [wt.%]	$d_{TS}/2$ [Å]	ξ_{TS} [Å]	S/V [Å^{-1}]
14	5	103	107	0.017
21	5	68	70	0.030
28	0	42	43	0.040

From the high q region, the specific interface S/V is accessible by using bulk and film contrast contributions according to Strey et al.[29] A more detailed discussion can be found in the Supporting Information. In accordance with the decreasing surfactant concentration and the corresponding larger domain size, the specific interface decreases from 0.040 Å^{-1} at $\gamma = 28$ wt% to 0.017 Å^{-1} at $\gamma = 14$ wt% (Table 3).

Based on the assumption that the catalyst complex is located in or near the surfactant film, which is supported by the observation that after phase separation due to the proceeding conversion of N-tosylamide **1** the oil excess phase was colourless while the microemulsion remained yellow, a decreasing surfactant concentration should increase the number of catalyst molecules per domain. Assuming that the volume of a domain can be described by a cube and considering the catalyst concentration of 10 µmol for $\gamma = 28$ wt% on average a catalyst molecule is present in every fifth domain. For the micro-

Chemistry–A European Journal

Full Paper
doi.org/10.1002/chem.202102752

Chemistry Europe
European Chemical
Societies Publishing

emulsions with larger domain size, the loading increases from 1 catalyst molecule at $\gamma = 21$ wt% towards 3 at $\gamma = 14$ wt%, which should result in a higher local concentration of the catalyst molecules at the specific interface and thus, higher yields.

Rh-catalyzed asymmetric 1,2-additions

In an initial screening different monomeric Rh-diene complexes [Rh(**L2**)X] (X = OTf, OTs, OAc PO₂F₂) and [Rh(**L2**)OH₂]SbF₆ were employed in the catalytic 1,2-addition of triphenylboroxine **2** to N-tosylimine **1** in the presence of 4 equiv. of 3.1 M KOH at 60 °C and a catalyst loading of 5 mol% (Table 4). Catalytic runs were performed both in dioxane and the previously used non-ionic microemulsion consisting of toluene, water and C₈G₁ at $\gamma = 28$ wt%.[17,18]

When Rh acetate [Rh(**L2**)OAc] was employed in dioxane only a meager NMR yield of 9% of the product **3** was detected and no attempts were made to isolate the product **3** and to determine the enantiomeric ratio (entry 1). In contrast, upon performing the catalysis in the non-ionic microemulsion the desired amine **3** was obtained in 52% NMR yield (e.r. 79:21) (entry 7). These results can be rationalized by the IBO calculations in the previous section (Table 2). The binding energy of the acetate is much higher than for the other anions and therefore the activation of the catalyst through the anion exchange of the acetate by a hydroxide anion is less favoured. The use of the microemulsion might facilitate the activation process and therefore lead to higher yields. The beneficial effect of the microemulsion on the yield was also observed for the Rh complexes with other anions (X = OTf, OTs, PO₂F₂) albeit at the expense of the enantiomeric ratio (entries 7–12). For example, [Rh(**L2**)OTf] gave 53% NMR yield (e.r. 93:7) in dioxane and 94% NMR yield (e.r. 84:16) in the microemulsion (ME) (entries 2, 8). Similar observations were made for [Rh(**L2**)OTs] (dioxane: 59%,

e.r. 90:10; ME: 93%, e.r. 67:33) (entries 3, 9) and [Rh(**L2**)PO₂F₂] (dioxane: 54%, e.r. 99:1; ME: 89%, e.r. 70:30) (entries 4, 10). A slightly different behavior was found for [Rh(**L2**)OH₂]SbF₆ bearing a weakly coordinating anion. The yield in the microemulsion was only slightly larger in dioxane while the selectivity was moderately lowered (dioxane: 51%, e.r. 96:4; ME: 56%, e.r. 85:15) (entries 5, 11). Similarly, for the corresponding benchmark dimeric complex [Rh(**L2**)Cl]₂ a slight increase of yield and a moderate decrease of enantioselectivity was observed in the microemulsion (73%, e.r. 93:7) as compared to dioxane (58%, for example 99:1) (entries 6, 12).[17] The improved yield obtained in the microemulsion is most likely related to the advantageous activation of the Rh complexes, which due to their amphiphilic structure, might preferentially reside at the huge interface of the amphiphilic film in comparison to the rather small macroscopic dioxane/KOHₐq interface. However, the explanation for the reduced enantioselectivities in the microemulsions is more complex. To investigate whether the chiral sugar surfactant C₈G₁ is responsible for the change in enantioselectivity a catalysis with the achiral rhodium complex [Rh(COD)Cl]₂ was carried out in the microemulsion (entry 13). In this experiment a racemic mixture of tosylamide **3** was obtained, proving that C₈G₁ itself does not induce enantioselectivity in the 1,2-addition.

To study the impact of electrostatic interactions between the charged catalyst and surfactant film on the catalytic reaction, microemulsions containing the non-ionic C₈G₁ carbohydrate surfactant and an anionic or cationic co-surfactant were employed in the asymmetric 1,2-addition. As anionic co-surfactants SDS and AOT were used, whereas DTAB was used as cationic co-surfactant. In a series of catalytic reactions [Rh(**L1**)Cl], [Rh(**L2**)Cl]₂, [Rh(**L2**)X] (X = OAc, OTs, OTf) and [Rh(**L2**)OH₂]SbF₆ were employed in microemulsions with different compositions of C₈G₁ and anionic co-surfactants (Table S7–S9). As expected from the high binding energy of the acetate

Table 4. Initial screening of the Rh-catalyzed 1,2-addition in dioxane and in a microemulsion (ME 1) with rhodium catalysts bearing different counterions.

Entry	Catalyst	Solvent	NMR yield [%][a]	Yield [%][b]	e.r. (R):(S)
1	[Rh(**L2**)OAc]	dioxane	9	n. d.	n. d.
2	[Rh(**L2**)OTf]	dioxane	53	53	93:7
3	[Rh(**L2**)OTs]	dioxane	59	56	90:10
4	[Rh(**L2**)PO₂F₂]	dioxane	54	47	99:1
5	[Rh(**L2**)OH₂]SbF₆	dioxane	51	45	96:4
6	[Rh(**L2**)Cl]₂	dioxane	58	55[17]	99:1
7	[Rh(**L2**)OAc]	C₈G₁-ME[c]	52	32	79:21
8	[Rh(**L2**)OTf]	C₈G₁-ME[c]	94	78	84:16
9	[Rh(**L2**)OTs]	C₈G₁-ME[c]	93	79	67:33
10	[Rh(**L2**)PO₂F₂]	C₈G₁-ME[c]	89	73	70:30
11	[Rh(**L2**)OH₂]SbF₆	C₈G₁-ME[c]	56	50	85:15
12	[Rh(**L2**)Cl]₂	C₈G₁-ME[c]	73	59[17]	93:7
13	[Rh(COD)Cl]₂	C₈G₁-ME[c]	>99	>99	50:50

[a] The progress of the reactions was monitored by ¹H NMR spectroscopy using mesitylene as an external standard. [b] Isolated yields. [c] C₈G₁-ME: Consisting of 0.60 g C₈G₁, 0.80 mL toluene and 0.70 mL H₂O at $\gamma = 28$ wt%.

Chemistry–A European Journal

Full Paper
doi.org/10.1002/chem.202102752

Chemistry Europe
European Chemical
Societies Publishing

anion compared to the other anions (see discussion above), the strongest influence of the microemulsion composition on the yield and selectivity was observed when [Rh(**L2**)OAc] was used as catalyst. Therefore, we focused our further studies on asymmetric 1,2-additions catalyzed by the acetate complex (Table 5).

Before studying the effect of a charged surfactant film on the 1,2-addition, the role of the presence of a microemulsion phase, and thus a nanoscale interfacial film, on the catalysis was examined. As a starting point toluene was chosen as an alternative solvent. However, when the 1,2-addition was performed in toluene no formation of *N*-tosylamide **3** was observed, and thus even less than in dioxane (9%) (entries 1 and 2). Subsequently, the catalysis was performed in a mixture of water and toluene with the addition of low amounts of C_8G_1 surfactant, i.e. at $\gamma = 2$ wt%, which is clearly above the CMC (note that in pure H_2O the CMC of C_8G_1 amounts to 0.6 wt% at $T = 40\,°C$).[33] At this composition the coexistence of a microemulsion with an excess water and oil phase is expected. Due to the presence of an amphiphilic film in the microemulsion phase, the NMR yield increased to 20% (entry 3). By increasing the C_8G_1 concentration to $\gamma = 8$ wt%, the volume of the microemulsion phase increases and thus a further improved yield and a surprisingly high enantioselectivity was observed (39%, e.r. 92:8) (entry 4). Note that for the one phase microemulsion at $\gamma = 28$ wt% a higher NMR yield but a lower enantioselectivity was obtained (52%, e.r. 79:21) (entry 5). The latter might be related to the higher concentration of reactants in the oil-rich domains of the single-phase microemulsion compared to the three-phase microemulsion.

Finally, we studied the effect of doping the non-ionic microemulsion on the 1,2-addition. At first, we replaced 5 wt% of C_8G_1 with the anionic SDS keeping the overall surfactant concentration constant at $\gamma = 28$ wt%. Interestingly, the yield increased to 70% at the expense of a lower enantioselectivity of e.r. 67:33 (entry 6). In the next step, the charge density of the amphiphilic film was further increased adjusting the concentration of SDS to $\delta_{SDS} = 10$ wt% keeping $\gamma = 28$ wt% constant (entry 7) resulting in a lower yield but a higher enantioselectivity (57%, e.r. 81:19). Here, the decreasing yield could be due to poorer activation of the catalyst because of electrostatic repulsion between the dissociated SDS^- and OH^-. Then, to study the influence of the size of water/oil domains the catalysis was performed at a lower C_8G_1/SDS concentration of $\gamma = 14$ wt% keeping δ_{SDS} constant at 10 wt% (entry 8). The observed larger yield of 74% and the lower enantioselectivity of e.r. 65:35 might be related to the higher catalyst loading of the larger domains with Rh-catalyst and to the decreasing order of the amphiphilic film due to size-dependent thermal fluctuations, respectively.

In the next series of experiments the anionic single-tailed co-surfactant SDS was replaced with AOT - an anionic surfactant with two branched tails (entries 9–11). In general, the use of AOT led to a strong increase of the enantioselectivity. For example the catalysis at $\gamma = 14$ wt% and $\delta_{AOT} = 5$ wt% yielded 63% of the *N*-tosylamide **3** with an e.r. of 95:5 (entry 9). Thereby, both yield and enantioselectivity stayed almost constant when the surfactant concentration was increased to $\gamma = 21$ wt% and $\gamma = 28$ wt% (entries 10 and 11). This observation differs from the catalytic reactions performed in the micro-

Table 5. Variation of the microemulsion for the Rh-catalyzed 1,2-addition with [Rh(**L2**)OAc].

Entry	Solvent	γ [wt. %]	δ [wt. %]	NMR yield [%][a]	Yield [%][b]	e.r. (R) : (S)
1	dioxane	–	–	9	n. d.	n. d.
2	toluene	–	–	0	–	–
3	toluene, water, C_8G_1[c]	2	–	20	n. d.	n. d.
4	toluene, water, C_8G_1[d]	8	–	39	35	92:8
5	C_8G_1-ME[e]	28	0	52	32	79:21
6	C_8G_1/SDS-ME[f]	28	5	70	65	67:33
7	C_8G_1/SDS-ME[g]	28	10	57	50	81:19
8	C_8G_1/SDS-ME[h]	14	10	74	70	65:35
9	C_8G_1/AOT-ME[i]	14	5	63	61	95:5
10	C_8G_1/AOT-ME[j]	21	5	56	50	94:6
11	C_8G_1/AOT-ME[k]	28	5	59	55	93:7
12	C_8G_1/DTAB-ME[l]	28	10	39	34	97:3

[a] The progress of the reactions was monitored by ^1H NMR spectroscopy using mesitylene as an external standard. [b] Isolated yields. [c] Addition of 2.93 mg C_8G_1 (half of the critical micellar concentration). [d] Addition of 11.7 mg C_8G_1 (twice the critical micellar concentration). [e] C_8G_1-ME: Consisting of 0.600 g C_8G_1, 0.80 mL toluene and 0.70 mL H_2O. [f] C_8G_1/SDS-ME: Consisting of 0.570 g C_8G_1, 0.030 g SDS, 0.80 mL toluene and 0.70 mL H_2O. [g] C_8G_1/SDS-ME: Consisting of 0.540 g C_8G_1, 0.060 g SDS, 0.80 mL toluene and 0.70 mL H_2O. [h] C_8G_1/SDS-ME: Consisting of 0.270 g C_8G_1, 0.030 g SDS, 0.98 mL toluene and 0.85 mL H_2O. [i] C_8G_1/AOT-ME: Consisting of 0.285 g C_8G_1, 0.015 g AOT, 0.98 mL toluene and 0.85 mL H_2O.[j] C_8G_1/AOT-ME: Consisting of 0.426 g C_8G_1, 0.022 g AOT, 0.90 mL toluene and 0.78 mL H_2O.[k] C_8G_1/AOT-ME: Consisting of 0.570 g C_8G_1, 0.030 g AOT, 0.80 mL toluene and 0.70 mL H_2O. [l] C_8G_1/DTAB-ME: Consisting of 0.540 g C_8G_1, 0.060 DTAB, 0.80 mL toluene and 0.70 mL H_2O.

Chemistry–A European Journal

Full Paper
doi.org/10.1002/chem.202102752

Chemistry Europe
European Chemical
Societies Publishing

emulsions doped with SDS and reveals the beneficial effect of AOT as compared to SDS.

In a final experiment the anionic AOT co-surfactant was exchanged with cationic DTAB to study, whether an inversely charged amphiphilic film has a different influence on the performance of the catalytic reaction (entry 12). Under these conditions a poor yield but the highest enantioselectivity was observed (39%, e.r. 97:3).

To rationalize the influence of the co-surfactant on the performance of the acetate catalyst a series of control experiments was carried out (Table 6).

First, the 1,2-addition with [Rh(**L2**)OAc] was examined in dioxane in the presence of 5 mol% of SDS (entry 1). Only a low yield of 7% of the product **3** was obtained, which agrees with the above discussed experiments in the absence of co-surfactant (Table 5). Next, the catalysis was performed with 52 mol% of SDS, which is similar to the amount of SDS used in the microemulsions in Table 5, resulting in an even lower yield of 4% (entry 2). By replacing dioxane with toluene/water and adding 5 mol% of SDS the yield could be improved to 20% and a high enantioselectivity (e.r. 96:4) was detected (entry 3). Upon using a larger amount of SDS (52 mol%) neither yield nor enantioselectivity changed much (entry 4).[34] When the 1,2-additions were run in dioxane in the presence of AOT similar observations were made as compared to SDS (entries 5,6). However, in toluene/water in the presence of AOT yields and enantioselectivities increased (entries 7,8). These results suggested that the increased yields in the microemulsions in Table 5 originated from the confinement provided by the nanodomains of the microemulsion. It should be noted, however that there is no simple correlation with the domain size. Larger domains (Table 3 and Table 5, entries 9–11) resulted in slightly larger yields and enantioselectivities, presumably due to the increased number of catalysts per domain. In addition, the increased enantioselectivity in the microemulsions (with co-surfactants) is probably due to exchange of acetate by the co-surfactant anion, as it was already visible in the biphasic toluene/water mixtures in Table 6.

To clarify whether an anion exchange takes place when AOT or SDS are added to [Rh(**L2**)OAc] a series of NMR experiments was carried out. For this purpose [Rh(**L2**)OAc] was dissolved either in dioxane or in a mixture of toluene and water, 1.0 equiv. of the respective co-surfactant was added and the reaction mixtures were stirred for 30 min at room temperature. For the experiments in dioxane the solvent was evaporated and the crude product was taken up in CDCl$_3$ while for the biphasic mixtures of toluene and water the organic phase was decanted prior to evaporation of the solvent. Finally, the ^{1}H NMR spectra were compared to the ^{1}H NMR spectra of the acetate complex and the co-surfactants (Figure 7 and Figure 8).

When [Rh(**L2**)OAc] was stirred with AOT or SDS in dioxane no anion exchange was observed in the ^{1}H NMR spectrum of the crude product and the acetate signal was still visible (Figure 7, (c) and Figure 8, (b)). The situation changed significantly when dioxane was replaced with a mixture of water and toluene. In this case, for both SDS and AOT a quantitative anion exchange was observed and no acetate signal was found in the NMR spectra of the crude products (Figure 7, (d) and Figure 8, (c)).

In addition equilibrium constants were calculated for the anion exchange of the acetate anion in [Rh(**L2**)OAc] with the investigated co-surfactants SDS and AOT. For the anion exchange with SDS a value of 7.00E-04 was found while it was 1.10E-03 for the anion exchange with AOT (for details see section 7.1, Supporting Information). These values indicate that the equilibrium is strongly shifted towards the reactants' side for both surfactants. This finding fits the weaker bond strength for the bond between the Rh and the surfactants compared to the bond between the Rh and the acetate as counterion, resulting in a missing driving force for the anion exchange (Table 2). Therefore, these theoretical calculations support the NMR studies that an anion exchange with the co-surfactants is unlikely in dioxane due to the lower binding energy of the co-surfactant anions to the Rh as compared to the Rh–OAc bond.

In contrast, according to the NMR studies anion exchange with the co-surfactants is favourable in toluene/water (It should be noted that the anion exchange equilibrium could not be

Table 6. Rh-catalyzed 1,2-addition with [Rh(**L2**)OAc] in dioxane and biphasic toluene-water mixtures with AOT and SDS additive.

Entry	Solvent	co-surfactant [mol%]	γ [wt.%]	NMR yield [%][a]	Yield [%][b]	e.r. (R):(S)
1	dioxane, SDS	5	0.16	7	n. d.	n. d.
2	dioxane, SDS	52	1.66	4	n. d.	n. d.
3	toluene, water, SDS	5	0.35	20	18	96:4
4	toluene, water, SDS	52	3.50	17	15	97:3
5	dioxane, AOT	5	0.25	8	n. d.	n. d.
6	dioxane, AOT	34	1.66	5	n. d.	n. d.
7	toluene, water, AOT	5	0.53	27	26	97:3
8	toluene, water, AOT	34	3.50	35	30	98:2

[a] The progress of the reactions was monitored by ^{1}H NMR spectroscopy using mesitylene as an external standard. [b] Isolated yields.
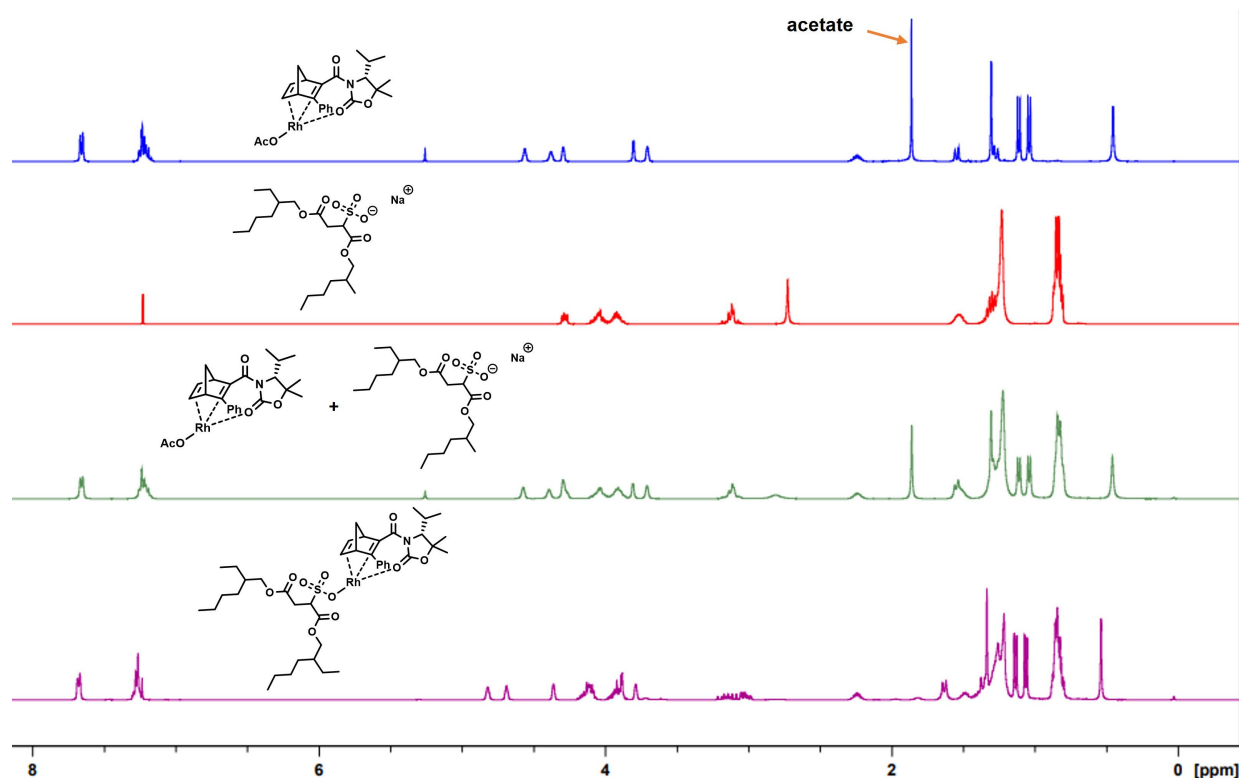
Chemistry–A European Journal

Full Paper
doi.org/10.1002/chem.202102752

Chemistry
Europe

European Chemical
Societies Publishing

Figure 7. ^{1}H NMR spectra of the anion exchange experiments with [Rh(**L2**)OAc] and AOT in dioxane (c) and in toluene/H₂O (d). For comparison the ^{1}H NMR spectra of [Rh(**L2**)OAc] (a) and AOT (b) are shown. All spectra were measured in CDCl₃ (400 MHz).

calculated for the toluene/water mixture since solvent mixtures cannot be treated with the used implicit solvation model). Presumably, the higher solubility of acetate in the aqueous phase shifts the equilibrium towards [Rh(**L2**)SDS] or [Rh(**L2**)AOT] respectively. Particularly the decreased binding energy of Rh–AOT and Rh–SDS as compared to Rh–OAc might lead to an accelerated reaction towards the catalytically active Rh–OH complex. Thus, the large interfacial area provided by the microemulsion and the accelerated formation of the active hydroxo catalyst result in increased yields.

Not only the yield, but also the enantioselectivity is strongly influenced by the properties of the co-surfactant. In order to rationalize this outcome, we propose the following model for the catalysis in microemulsions with anionic co-surfactants (Figure 9).

Due to the sterically demanding branched alkyl chains of the AOT⁻ anion in [Rh(**L2**)AOT] an interdigitation[35] with the hydrophobic tails of the surfactants in the amphiphilic film might be disfavoured (Figure 9, (a)), in contrast to the unbranched SDS⁻ tail of [Rh(**L2**)SDS], which fits better into the layer of hydrophobic alkyl chains (Figure 9, (b)). Additionally, the polarity of AOT is lower than SDS, which leads to higher solubility in toluene. Therefore, the [Rh(**L2**)AOT] complex should rather be located at the periphery of the amphiphilic film near the toluene domains.Thus, we assume that the enantioselectivity depends strongly on the chemical environment of the complex. In case of the 1,2-addition in C₈G₁/SDS microemulsion

the surfactants in the amphiphilic film might disturb the catalyst, which leads to lower enantioselectivities (see Table 5, entries 6–8). In contrast, [Rh(**L2**)AOT] resides closer to the toluene domains and is not disturbed by additional surfactant molecules. This agrees well with the high enantioselectivities obtained for C₈G₁/AOT microemulsions (see Table 5, entries 9–11).

Kinetics of the 1,2-addition in different solvents

For a deeper understanding of the influence of the micro-emulsions on the Rh-catalyzed 1,2-addition a series of kinetic experiments was performed. Therefore, the previously investigated acetate complex [Rh(**L2**)OAc] was chosen as catalyst and the temperature dependence of the kinetics in the pure C₈G₁ microemulsion (ME 1 at $T=60\,°C$: □, ME 1 at $T=50\,°C$: ▽; ME 1 at $T=40\,°C$: ○) was studied and compared to the kinetics in dioxane at $60\,°C$ (◇) (Figure 10).

Kinetics in dioxane at $T=60\,°C$ were very sluggish and a maximum NMR yield of 6% was reached. The microemulsion tremendously increased the NMR yield and the 1,2-addition was significantly accelerated. Kinetics were significantly slower at $40\,°C$ and $50\,°C$ as compared to the kinetics at $60\,°C$. However, the final NMR yield was higher when the reaction was performed at $40\,°C$ or $50\,°C$ ($T=40\,°C$: 78%; $T=50\,°C$: 71%; $T=60\,°C$: 67%). This behaviour indicates that the side reactions

Chemistry–A European Journal

Full Paper
doi.org/10.1002/chem.202102752

Chemistry
Europe
European Chemical
Societies Publishing

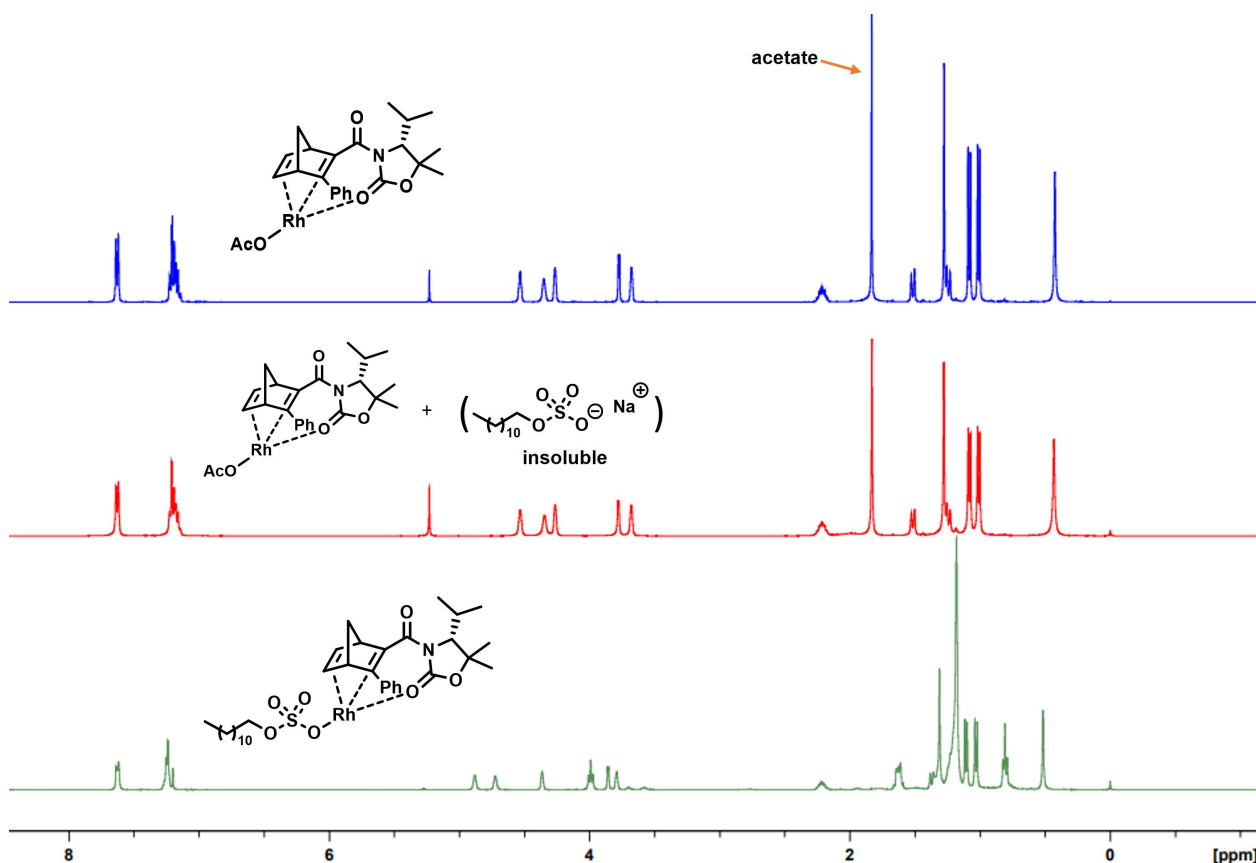**Figure 8.** Crude ^{1}H NMR spectra of the anion exchange experiments with [Rh(**L2**)OAc] and SDS in dioxane (b) and in toluene/H$_2$O (c). For comparison the ^{1}H NMR spectrum of [Rh(**L2**)OAc] (a) is shown. All spectra were measured in CDCl$_3$ (400 MHz).

(Scheme 3) have a higher activation energy in comparison to the formation of the *N*-tosylamine **3** and become thus more dominant at higher temperatures.

Hydrolysis of *N*-tosylimine **1** at higher temperature leads to the formation of the aldehyde **4** which then reacts in a Rh-catalyzed 1,2-addition to irreversibly form the alcohol **6**. The alcohol **6** is frequently observed in the ^{1}H NMR of crude products as described in our previous publication.[18]
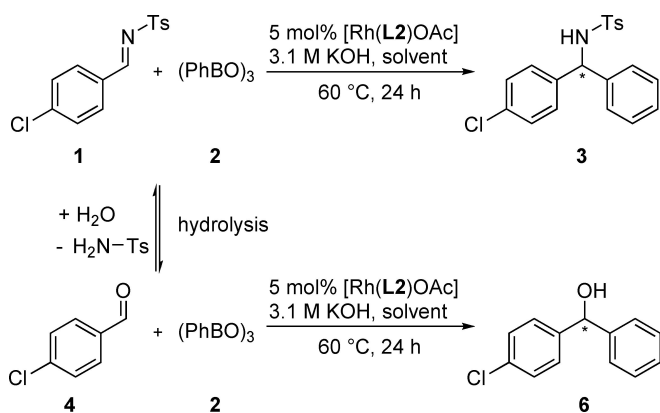
Scheme 3. Side reactions in the Rh-catalyzed 1,2-addition of *N*-tosylimine **1** and triphenyl-boroxine **2**.

Interestingly, when the fraction of newly formed product was plotted as a function of time in a double logarithmic plot, a linear behavior was observed (see Figure S33, Supporting Information). This power law behavior suggests that several processes contribute to the kinetics.[36] Accordingly, a reasonable description of the formation of *N*-tosylamide **3** is given by

$$\text{yield } (t) = A_{t\to\infty} - A_{t\to\infty}(t/t_0)^{-m}$$

Here $A_{t\to\infty}$ corresponds to the final yield, t_0 to an effective reciprocal rate constant and m to the power, determined from the slope of the log-log plot. As can be seen, the power law describes the experimental data almost quantitatively. From the analysis, a systematic decrease of t_0 with increasing temperature was observed. Interestingly, the value of the power m was found to be not constant, but exhibits different values for the three temperatures (see Supporting Information); the reason for this variation of m will be investigated in the future.

Subsequently, kinetic measurements were carried out at 50 °C since [Rh(**L2**)OAc] varying the surfactant mass fraction γ. In more detail, the following reaction media were chosen: water, toluene, C$_8$G$_1$ (γ = 8 wt%, ▽), ME 5 (γ = 14 wt%, δ$_{AOT}$ = 5 wt%, ○), ME 6 (γ = 21, δ$_{AOT}$ = 5 wt%, △), ME 7 (γ = 28 wt%, δ$_{AOT}$ = 5 wt%, □) (Figure 11, for further details see Table 5). As

Chemistry–A European Journal

Full Paper
doi.org/10.1002/chem.202102752

Chemistry
Europe
European Chemical
Societies Publishing
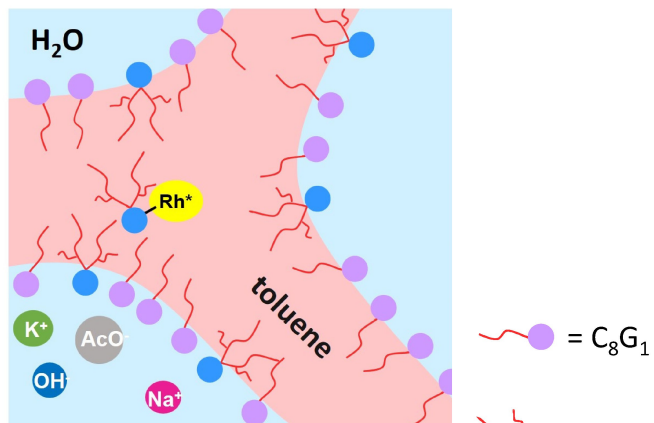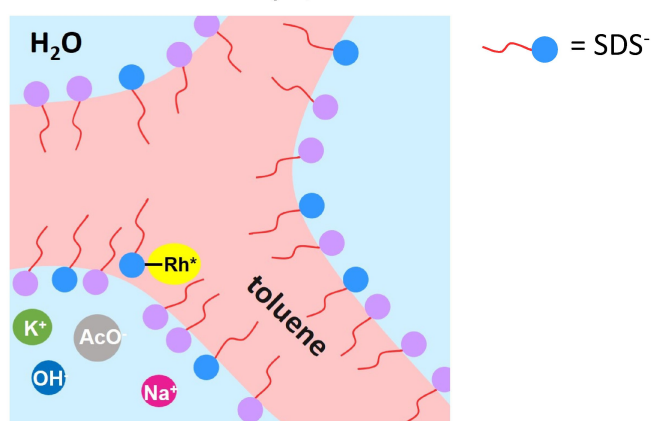
Figure 9. Proposed location of (a) [Rh(L2)AOT] in a C_8G_1/AOT microemulsion and (b) [Rh(L2)SDS] in a C_8G_1/SDS microemulsion.

Figure 10. Temperature dependency of the Rh-catalyzed 1,2-addition with [Rh(L2)OAc] in the C_8G_1 microemulsion ($\gamma = 28$ wt%, for further details of the C_8G_1-ME composition see Table 5). The data was described by a power law approach.

in the study of temperature influence, the obtained data were described by the power law approach.

When the catalysis was performed in a three-phase mixture of water, toluene and $\gamma = 8$ wt% of C_8G_1 the kinetics were slow and only 34% yield of N-tosylamine 3 were reached. This observation can be explained by the smaller interfacial area, as the microemulsion phase coexists with large micrometer-sized emulsion droplets of the excess water and oil phase. The two latter will lead to increasing diffusion paths of both the two reactants as well as OH⁻ to the rhodium catalyst. When the AOT doped microemulsions were applied as reaction media both kinetics and the overall NMR yield significantly increased. For catalysis performed in one-phase microemulsions similar effective reciprocal rate constant were observed varying the surfactant mass fraction from $\gamma = 28$ wt%, □ over $\gamma = 21$ wt%, Δ to $\gamma = 14$ wt% at $\delta_{AOT} = 5$ wt% (○). This finding may arise from a compensation of the decreasing specific interface S/V determined by SAXS analysis (see Table 3) and the increasing number of catalyst molecules in the latter. Note that the number of catalyst molecules is kept constant in all samples. The slight increase in yield observed with decreasing surfactant mass fractions (also surmisable in catalysis performed at
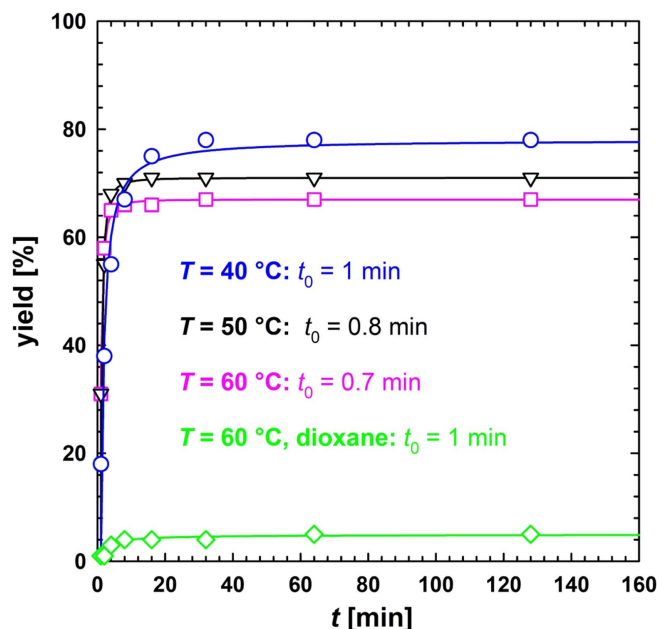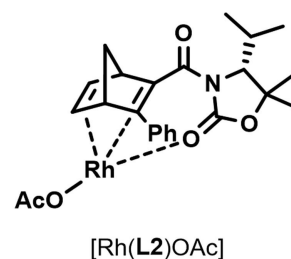
$T = 60$ °C, Table 5) is most probably related to the increase in local catalyst concentration at the specific interface.

Conclusion

The use of microemulsions as reaction media is a promising alternative for catalytic reactions as compared to conventional organic solvents. Microemulsions (a) provide defined reaction spaces due to their nanostructured domains, (b) provide a large interfacial area which can be useful to overcome diffusion limitations and (c) the polarity of the amphiphilic film can be adjusted by the proper choice of surfactants. To investigate the influence of these effects on asymmetric catalysis a series of chiral Rh norbornadiene complexes [Rh(L2)X] (X=OTf, OTs, OAc, PO_2F_2) and [Rh(L2)OH₂]SbF₆ bearing different counterions were synthesized. X-ray crystallographic data and theoretical calculations revealed increasing Rh–X binding energies in the series (including the co-surfactant anions SDS⁻ and AOT⁻): Rh–AOT = Rh–OTf < Rh–SDS = Rh–PO₂F₂ < Rh–OTs < Rh–OAc, i.e. the AcO⁻ counterion was bound more than 100 kJ/mol stronger to the Rh than TfO⁻ or AOT⁻.
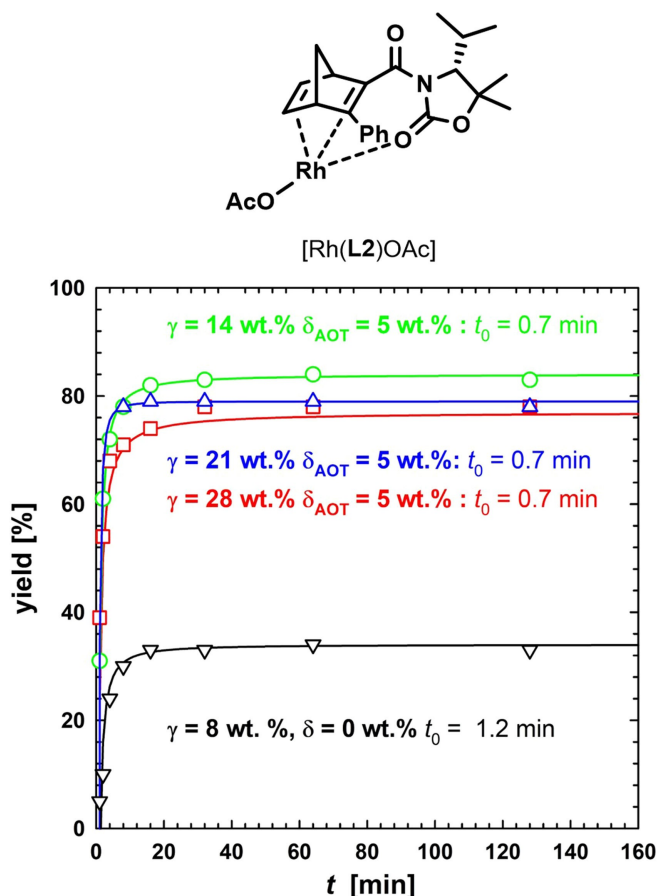
Chemistry–A European Journal

Full Paper
doi.org/10.1002/chem.202102752

Chemistry Europe
European Chemical
Societies Publishing

Figure 11. Kinetics of the Rh-catalyzed 1,2-addition with [Rh(**L2**)OAc] in AOT-doped C_8G_1 microemulsions with varying γ values at 50 °C. The data was described by a power law approach.

In order to answer the question whether and how the interaction of a charged catalyst with the amphiphilic surfactant film effects the yield and selectivity of the Rh-catalyzed asymmetric 1,2-addition of triphenylboroxine **2** to *N*-tosylimine **1**, the non-ionic sugar surfactant C_8G_1 was partially replaced by the anionic surfactants sodium dodecyl sulfate (SDS), dioctyl sodium sulfosuccinate (AOT) and the cationic surfactant dodecyl trimethyl ammonium bromide (DTAB). The phase behaviour of these nanostructured reaction media was thoroughly investigated by recording $T(\gamma)$-sections through the phase space. The doping with small amounts of SDS and AOT enabled a significant enhancement of the surfactant mixture efficiency to solubilize water and oil, which resulted from the electrostatic stiffening of the amphiphilic film and due to the reduction of thermal fluctuations. However, increasing the co-surfactant concentration further, at a certain point a decrease of the efficiency was observed most probably related to the decreasing distance between the surfactant headgroups and the increasing number of Na^+ counterions. Note that by doping with DTAB the efficiency initially decreased before it became slightly more efficient than the non-doped microemulsion most probably due a lower degree of dissociation compared to SDS and AOT. Furthermore, the domain size and the specific

interface were determined by SAXS experiments exemplary performed at the European Synchrotron Radiation Facility (ESRF, Grenoble, France) by means of selected microemulsions doped with AOT. The quantitative analysis of the scattering curves revealed that the domain size increases from 42 Å to 103 Å when the surfactant concentration is decreased from 28 wt% to 14 wt%, while the specific interface decreases from 0.040 Å⁻¹ to 0.017 Å⁻¹, respectively.

Employing the C_8G_1 microemulsion in the catalytic asymmetric 1,2-addition of triphenylboroxine **2** to *N*-tosylimine **1** in the presence of [Rh(**L2**)X] revealed a significant anion-dependent increase of the catalytic activity as compared to dioxane. The largest effect was observed for [Rh(**L2**)OAc] (9% yield in dioxane vs. 52% in C_8G_1-ME). Regarding the enantioselectivity decreased values were obtained for [Rh(**L2**)X] in the C_8G_1 microemulsion as compared to dioxane, which is in agreement with previous studies on Rh–Cl complexes.[18]

Since the C_8G_1 microemulsion had the highest impact on the catalytic activity of [Rh(**L2**)OAc], subsequent experiments focused on the question whether and how the interaction of a charged catalyst with the amphiphilic surfactant film effects the yield and selectivity of the reaction. Using the microemulsions doped with co-surfactants both yield and enantioselectivity could be tailored by the choice of the co-surfactant. Regarding yields the following trend was observed: SDS > AOT > DTAB, while enantioselectivities followed the opposite trend: DTAB > AOT > SDS. For AOT larger domains of the microemulsions resulted in slightly higher yield and enantioselectivities due to larger number of catalysts per domain. NMR experiments, theoretical calculations and catalytic studies with solvent/co-surfactant mixtures revealed the unique roles of the counterion and type of co-surfactant. The data indicated that the anion exchange AcO^- vs. SDS^-, AOT^- accelerated the formation of the catalytically active Rh-OH complex and thus increased the yield.

The high enantioselectivities observed in one-phase microemulsions with AOT agreed well with the results in biphasic toluene/H_2O with small amount of AOT, in contrast to microemulsions with SDS where much lower enantioselectivities were detected. The different behavior of AOT and SDS might be rationalized by their different location in the amphiphilic film.

Kinetic studies of the catalysis with [Rh(**L2**)OAc] revealed cleaner reactions at lower temperatures, indicating that the side reactions, i.e. the hydrolysis of *N*-tosylimine **1** and the competing 1,2-addition to the aldehyde **4** have a higher activation energy. The analysis of the data by a power law approach revealed that the effective reciprocal reaction rate decreases slightly when temperature decreases. Furthermore, a compensative effect of the decreasing specific interface *S/V* and the increasing number of catalyst molecules with decreasing surfactant mass fraction results in an almost constant effective reciprocal reaction rate.

In conclusion, microemulsions doped with ionic co-surfactants are valuable ordered reaction media for asymmetric Rh diene catalysis, particularly when the polarity of the Rh complex can be tailored via the Rh–X bond. Future work must demonstrate the extension of this concept for other transition metal catalysts.

Chemistry–A European Journal

Full Paper
doi.org/10.1002/chem.202102752

Chemistry Europe
European Chemical
Societies Publishing

Experimental Section

Full details of synthetic procedures and characterization data, NMR spectra, mass spectra, FTIR spectra, X-ray crystallographic data, microemulsion characterization data, SAXS measurements, HPLC chromatograms, analysis of kinetics, as well as the DFT computational details can be found in the Supporting Information.

Deposition Number(s) 2099413 ([Rh(**L2**)OTf]), 2099414 ([Rh(**L2**)OTs]), 2099419 ([Rh(**L2**)OAc]), 2099420 ([Rh(**L2**)PO$_2$F$_2$]), 2099421 ([Rh(**L2**)OH$_2$]SbF$_6$·CH$_2$Cl$_2$) contain(s) the supplementary crystallographic data for this paper. These data are provided free of charge by the joint Cambridge Crystallographic Data Centre and Fachinformationszentrum Karlsruhe Access Structures service.

Conflict of Interest

The authors declare no conflict of interest.

[1] a) A. Steinhaus, D. Srivastva, X. Qiang, S. Franzka, A. Nikoubashman, A. H. Groeschel, *Macromolecules* **2021**, *54*, 1224–1233; b) X. Dai, X. Qiang, C. Hils, H. Schmalz, A. H. Groeschel, *ACS Nano* **2021**, *15*, 1111–1120; c) L. Schneider, G. Lichtenberg, D. Vega, M. Mueller, *ACS Appl. Mater. Interfaces* **2020**, *12*, 50077–50095; d) B. Kuttich, I. Hoffmann, B. Stuehn, *Soft Matter* **2020**, *16*, 10377–10385; e) A. E. L. Aferni, M. Guettari, T. Tajouri, A. Rahdar, *J. Mol. Liq.* **2020**, *318*, 114012; f) Y. Alqarni, F. Ishizuka, T. D. M. Bell, R. F. Tabor, P. B. Zetterlund, K. Saito, *Polym. Chem.* **2020**, *11*, 4326–4334; g) Y. Kim, J. Mun, G. Yu, K. Char, *Macromol. Res.* **2017**, *25*, 656–661.

[2] a) J. H. Koo, D. Kim, J. G. Kim, H. Jeong, J. Kim, I. S. Lee, *Nanoscale* **2016**, *8*, 14593–14599; b) Y. Tian, W. Luo, Y. Wang, Y. Yu, W. Huang, H. Tang, Y. Zheng, Z. Liu, *Ultrason. Sonochem.* **2021**, *73*, 105484; c) E. T. Adesuji, V. O. Torres-Guerrero, J. A. Arizpe-Zapata, M. Videa, M. Sanchez-Dominguez, K. M. Fuentes, *Nanotechnology* **2020**, *31*, 425601; d) J. Yin, J. Yu, X. Shi, W. Kong, Z. Zhou, J. Man, J. Sun, Z. Wen, *J. Colloid Interface Sci.* **2021**, *582*, 874–882; e) Q. Wang, K. S. Hernesman, O. Steinbock, *ChemSystemsChem* **2020**, *2*, e1900037; f) K. Jia, J. Xie, X. He, D. Zhang, B. Hou, X. Li, X. Zhou, Y. Hong, X. Liu, *Chem. Eng. J.* **2020**, *395*, 125123; g) Z. Cong, B. Lin, W. Li, J. Niu, F. Yan, *J. Nanosci. Nanotechnol.* **2018**, *18*, 7917–7922; h) Y. Liu, K. Lan, S. Li, Y. Liu, B. Kong, G. Wang, P. Zhang, R. Wang, H. He, Y. Ling, A. M. Al-Enizi, A. A. Elzatahry, Y. Cao, G. Chen, D. Zhao, *J. Am. Chem. Soc.* **2017**, *139*, 517–526.

[3] a) F. C. Meldrum, C. O'Shaughnessy, *Adv. Mater.* **2020**, *32*, 2001068; b) A. Scano, V. Cabras, M. Pilloni, G. Ennas, *J. Nanosci. Nanotechnol.* **2019**, *19*, 4824–4838; c) M. Sanchez-Dominguez, K. Pemartin, C. Solans, M.

Boutonnet, *Adv. Colloid Interface Sci.* **2014**, *4*, 177–197; d) M. Sanchez-Dominguez, C. Aubery, C. Solans, *Smart Nanoparticles Technology* (Ed.: A. A. Hashim), InTech, Rijeka **2012**, ch. 9; e) M. Sanchez-Dominguez, K. Pemartin, M. Boutonnet, *Curr. Opin. Colloid Interface Sci.* **2012**, *17*, 297–305; f) T. Aubert, F. Grasset, S. Mornet, E. Duguet, O. Cador, S. Cordier, Y. Molard, V. Demange, M. Mortier, H. Haneda, *J. Colloid Interface Sci.* **2009**, *341*, 201–208; g) M.-E. Meyre, C. Faure, *Recent Res. Dev. Phys. Chem.* **2004**, *7*, 321–338; h) D. G. Shchukin, G. B. Sukhorukov, *Adv. Mater.* **2004**, *16*, 671–682.

[4] J. Guo, Y. Zhang, Y. Zhu, C. Long, M. Zhao, M. He, X. Zhang, J. Lv, B. Han, Z. Tang, *Angew. Chem. Int. Ed.* **2018**, *57*, 6873–6877; *Angew. Chem.* **2018**, *130*, 6989–6993.

[5] O. Wrede, S. Grosskopf, T. Seidel, T. Hellweg, *Phys. Chem. Chem. Phys.* **2019**, *21*, 6725–6731.

[6] a) P. Weigl, V. Talluto, T. Walther, T. Blochowicz, *Z. Phys. Chem.* **2018**, *232*, 1017–1039; b) M. Pourtabrizi, N. Shahtahmassebi, A. Kompany, S. Sharifi, *J. Fluoresc.* **2018**, *28*, 323–336.

[7] a) Y. Feldman, A. Puzenko, Y. Ryabov, *Adv. Chem. Phys.* **2006**, *133*, 1–125; b) H. Kim, M. Han, S. R. Bandara, R. M. Espinosa-Marzal, C. Leal, *Soft Matter* **2019**, *15*, 9609–9613; c) B. Kuttich, A. Matt, A. Weber, A.-K. Grefe, L. Vietze, B. Stuehn, *Z. Phys. Chem.* **2018**, *232*, 1089–1110; C. Dutta, A. Svirida, M. Mammetkuliyev, M. Rukhadze, A. V. Benderskii, *J. Phys. Chem. B* **2017**, *121*, 7447–7454.

[8] a) M. Kahlweit, R. Strey, *Angew. Chem. Int. Ed.* **1985**, *24*, 654–668; *Angew. Chem.* **1985**, *97*, 655–659; b) T. Sottmann, R. Strey, *Fundamentals of Interface and Colloid Science: Microemulsions, Vol. 5* (Ed.: J. Lyklema), Elsevier, Amsterdam **2005**, ch. 5.1–5.96; c) R. Strey, *Colloid Polym. Sci.* **1994**, *272*, 1005–1019; d) T. Sottmann, R. Strey, S.-H. Chen, *J. Chem. Phys.* **1997**, *106*, 6483–6491.

[9] a) K. Holmberg, *Curr. Opin. Colloid Interface Sci.* **2003**, *8*, 187–196; b) T. Wielpütz, T. Sottmann, R. Strey, F. Schmidt, A. Berkessel, *Chem. Eur. J.* **2006**, *12*, 7565–7575; c) S. Serrano-Luginbühl, K. Ruiz-Mirazo, R. Ostaszewski, F. Gallou, P. Walde, *Nat. Chem. Rev.* **2018**, *2*, 306–327; d) I. Rico-Lattes, E. Perez, S. Franceschi-Messant, A. Lattes, *C. R. Chim.* **2011**, *14*, 700–715; e) M. Schwarze, T. Pogrzeba, I. Volovych, R. Schomäcker, *Catal. Sci. Technol.* **2015**, *5*, 24–33; f) M.-J. Schwuger, K. Stickdorn, R. Schomaecker, *Chem. Rev.* **1995**, *95*, 849–864; g) M. Schwarze, T. Pogrzeba, K. Seifert, T. Hamerla, R. Schomäcker, *Catal. Today* **2015**, *247*, 55–63; h) J. S. Milano-Brusco, H. Nowothnick, M. Schwarze, R. Schomäcker, *Ind. Eng. Chem. Res.* **2010**, *49*, 1098–1104; i) H. H. Y. Ünveren, R. Schomäcker, *Catal. Lett.* **2005**, *102*, 83–89; j) H. H. Y. Ünveren, R. Schomäcker, *Catal. Lett.* **2006**, *110*, 195–201; k) M. Haumann, H. Koch, P. Hugo, R. Schomäcker, *Appl. Catal. A* **2002**, *225*, 239–249; l) A. Rost, Y. Brunsch, A. Behr, R. Schomäcker, *Chem. Eng. Technol.* **2014**, *37*, 1055–1064; m) T. Yosef, R. Schomäcker, M. Schwarze, M. Fanun, F. Gelman, J. Blum, *J. Mol. Catal. A* **2011**, *351*, 46–51; n) Z. Nairoukh, M. Fanun, M. Schwarze, R. Schomäcker, J. Blum, *J. Mol. Catal. A* **2014**, *382*, 93–98; o) H. N. Kagalwala, D. N. Chirdon, I. N. Mills, N. Budwal, S. Bernhard, *Inorg. Chem.* **2017**, *56*, 10162–10171; p) M. Laupheimer, S. Engelskirchen, K. Tauber, W. Kroutil, C. Stubenrauch, *Tenside Surfactants Deterg.* **2011**, *48*, 28–33; q) M. Sathishkumar, R. Jayabalan, S. P. Mun, S. E. Yun, *Bioresour. Technol.* **2010**, *101*, 7834–7840; r) G. Hedström, M. Backlund, J. P. Slotte, *Biotechnol. Bioeng.* **1993**, *42*, 618–624; s) G. D. Rees, K. Carlile, G. E. Crooks, T. R.-J. Jenta, L. A. Price, B. H. Robinson in *Engineering of/ with Lipases* (Ed.: F. X. Malcata), Springer Netherlands, Dordrecht, **1996**, pp. 577–595; t) G. D. Rees, B. H. Robinson, G. R. Stephenson, *Biochim. Biophys. Acta* **1995**, *1259*, 73–81; u) S.-F. Song, Y.-X. Luan, *Chem. Res. Chin. Univ.* **2010**, *26*, 110–113.

[10] a) B. Nuthakki, J. M. Bobbitt, J. F. Rusling, *Langmuir* **2006**, *22*, 5289–5293; b) M. Schmidt, C. Urban, S. Schmidt, R. Schomäcker, *ACS Omega* **2018**, *3*, 13355–13364.

[11] a) S. Handa, D. J. Lippincott, D. H. Aue, B. H. Lipshutz, *Angew. Chem. Int. Ed.* **2014**, *53*, 10658–10662; *Angew. Chem.* **2014**, *126*, 10834–10838.

[12] M. Hejazifar, A. M. Palvoelgyi, J. Bitai, O. Lanaridi, K. Bica-Schroeder, *Org. Process Res. Dev.* **2019**, *23*, 1841–1851.

[13] D. Langevin, *Structure and Dynamics of Strongly Interacting Colloids and Supramolecular Aggregates in Solution* (Eds.: S.-H. Chen, J. S. Huang, P. Tartaglia), Springer Science & Business Media, **2012**, 325–350.

[14] M. Schmidt, J. Deckwerth, R. Schomäcker, M. Schwarze, *J. Org. Chem.* **2018**, *83*, 7398–7406.

[15] T. Pogrzeba, M. Schmidt, N. Milojevic, C. Urban, M. Illner, J.-U. Repke, R. Schomäcker, *Ind. Eng. Chem. Res.* **2017**, *56*, 9934–9941.

[16] I. Volovych, M. Neumann, M. Schmidt, G. Buchner, J.-Y. Yang, J. Wölk, T. Sottmann, R. Strey, R. Schomäcker, M. Schwarze, *RSC Adv.* **2016**, *6*, 58279–58287.

[17] M. Kirchhof, K. Gugeler, F. R. Fischer, M. Nowakowski, A. Bauer, S. Alvarez-Barcia, K. Abitaev, M. Schnierle, Y. Quawasmi, W. Frey, A. Baro, D. P. Estes, T. Sottmann, M. R. Ringenberg, B. Plietker, M. Bauer, J. Kästner, S. Laschat, *Organometallics* **2020**, *39*, 3131–3145.

[18] M. Deimling, M. Kirchhof, B. Schwager, Y. Qawasmi, A. Savin, T. Mühlhäuser, W. Frey, B. Claasen, A. Baro, T. Sottmann, S. Laschat, *Chem. Eur. J.* **2019**, *25*, 9464–9476.

[19] a) C. Defieber, H. Grützmacher, E. M. Carreira, *Angew. Chem. Int. Ed.* **2008**, *47*, 4482–4502; *Angew. Chem.* **2008**, *120*, 4558–4579; b) J. B. Johnson, T. Rovis, *Angew. Chem. Int. Ed.* **2008**, *47*, 840–871; *Angew. Chem.* **2008**, *120*, 852–884; c) R. M. Maksymowicz, A. J. Bissette, S. P. Fletcher, *Chem. Eur. J.* **2015**, *21*, 5668–5678; d) M. Nagamoto, T. Nishimura, *ACS Catal.* **2017**, *7*, 833–847.

[20] Selected examples: a) Y. Ichikawa, T. Nishimura, T. Hayashi, *Organometallics* **2011**, *30*, 2342–2348; b) D. Chen, X. Zhang, W.-Y. Qi, B. Xu, M.-H- Xu, *J. Am. Chem. Soc.* **2015**, *137*, 5268–5271; c) T. Nishimura, T. Katoh, K. Takatsu, R. Shintani, T. Hayashi, *J. Am. Chem. Soc.* **2007**, *129*, 14158–14159; d) B. Moku, W. Fang, J. Leng, E. A. B. Kantchev, H. Qin, *ACS Catal.* **2019**, *9*, 10477–10488; e) Y. Luo, H. B. Hepburn, N. Chotsaeng, H. W. Lam, *Angew. Chem. Int. Ed.* **2012**, *51*, 8309–8313; *Angew. Chem.* **2012**, *124*, 8434–8438; f) X. Ma, J. Jiang, S. Lv, W. Yao, Y. Yang, S. Liu, F. Xia, W. Hu, *Angew. Chem. Int. Ed.* **2014**, *53*, 13136–13139; *Angew. Chem.* **2014**, *126*, 13352–13355; g) D.-X. Zhu, H. Xia, J.-G. Liu, L. W. Chung, M.-H. Xu, *J. Am. Chem. Soc.* **2021**, *143*, 2608–2619; h) A. Selmani, S. Darses, *Org. Lett.* **2020**, *22*, 2681–2686.

[21] R. Fernández-Galán, B. R. Manzano, A. Otero, M. Lanfranchi, A. Pellinghelli, *Inorg. Chem.* **1994**, *33*, 2309–1312.

[22] M. G. Freire, C. M. S. S. Neves, I. M. Marrucho, J. A. P. Coutinho, A. M. Fernandes, *J. Phys. Chem. A* **2010**, *114*, 3744–3749.

[23] TURBOMOLE V7.1 **2016**, a development of University of Karlsruhe and Forschungszentrum Karlsruhe GmbH, **1989–2007**, TURBOMOLE GmbH, since **2007**.

[24] G. Knizia, *J. Chem. Theory Comput.* **2013**, *9*, 4834–4843.

[25] J. A. Silas, E. W. Kaler, *J. Colloid Interface Sci.* **2001**, *243*, 248–254.

[26] K. Peng, T. Sottmann, C. Stubenrauch, *Mol. Phys.* **2021**, e1886363.

[27] R. Schomäcker, R. Strey, *J. Phys. Chem.* **1994**, *98*, 3908–3912.

[28] M. Kahlweit, R. Strey, *J. Phys. Chem.* **1988**, *92*, 1557–1563.

[29] R. Strey, J. Winkler, L. Magid, *J. Phys. Chem.* **1991**, *95*, 7502–7507.

[30] M. Teubner, R. Strey, *J. Chem. Phys.* **1987**, *87*, 3195–3200.

[31] J. Schelten, W. Schmatz, *J. Appl. Crystallogr.* **1980**, *13*, 385–390.

[32] J. A. Silas, E. W. Kaler, *J. Colloid Interface Sci.* **2003**, *257*, 291–298.

[33] B. Arlt, S. Datta, T. Sottmann, S. Wiegand, *J. Phys. Chem. B* **2010**, *114*, 2118–2123.

[34] For related work on micellar Rh catalysis see: D. Motoda, H. Kinoshita, H. Shinokubo, K. Oshima, *Angew. Chem. Int. Ed.* **2004**, *43*, 1860–1862; *Angew. Chem.* **2004**, *116*, 1896–1898.

[35] M. Sammalkorpi, M. Karttunen, M. Haataja, *J. Am. Chem. Soc.* **2008**, *130*, 17777–17980.

[36] I. Grossman-Haham, G. Rosenblum, T. Namani, H. Hofmann, *Proc. Natl. Acad. Sci. USA* **2018**, *115*, 513–518.